HHS Public Access

Author manuscript

Curr Biol. Author manuscript; available in PMC 2020 November 18.

Published in final edited form as:

Curr Biol. 2019 November 18; 29(22): 3778–3790.e8. doi:10.1016/j.cub.2019.09.018.

The receptor kinases BAK1/SERK4 regulate Ca^{2+} channel-mediated cellular homeostasis for cell death containment

Xiao Yu[1,2,10], **Guangyuan Xu**[1,3,4,10], **Bo Li**[1,2,5], **Luciano de Souza Vespoli**[1,2], **Hai Liu**[6], **Wolfgang Moeder**[7], **Sixue Chen**[8], **Marcos V. V. de Oliveira**[1,3], **Suzane Ariádina de Souza**[1,2], **Wenyong Shao**[1,2], **Bárbara Rodrigues**[1,2], **Yi Ma**[9], **Shweta Chhajed**[8], **Shaowu Xue**[6], **Gerald A. Berkowitz**[9], **Keiko Yoshioka**[7], **Ping He**[1,3,4,*], **Libo Shan**[1,2,4,11,*]

[1]Institute for Plant Genomics & Biotechnology, Texas A&M University, College Station, TX 77843, USA

[2]Department of Plant Pathology & Microbiology, Texas A&M University, College Station, TX 77843, USA

[3]Department of Biochemistry & Biophysics, Texas A&M University, College Station, TX 77843, USA

[4]College of Plant Protection, China Agricultural University, Beijing, 100193, P. R. China

[5]Provincial Key Laboratory of Plant Pathology of Hubei Province, College of Plant Science and Technology, Huazhong Agricultural University, Wuhan, Hubei, 430070, P. R. China

[6]College of Life Science and Technology, Huazhong Agricultural University, Wuhan, Hubei, 430070, P. R. China

[7]Department of Cell and Systems Biology, Center for the Analysis of Genome Evolution and Function (CAGEF), University of Toronto, Toronto, ON, M5S 3B2, Canada

[8]Department of Biology, Genetics Institute, Plant Molecular and Cellular Biology Program, University of Florida, Gainesville, Florida 32610, USA

[9]Department of Plant Science and Landscape Architecture, University of Connecticut, Storrs, CT 06269, USA

[10]These authors contributed equally

[11]Lead Contact

SUMMARY

Cell death is a vital and ubiquitous process that is tightly controlled in all organisms. However, the mechanisms underlying precise cell death control remain fragmented. As an important shared

*Correspondence: lshan@tamu.edu (L.S), pinghe@tamu.edu (P.H).

AUTHOR CONTRIBUTIONS

X.Y., G.X., B.L., L.S., and P.H. conceived the project, designed experiments and analyzed data. X.Y., G.X., B.L., L.V., H.L., W.M., S.C., M.O., S.S., W.S., B.R., Y.M., and S.C. performed experiments and analyzed data. G.B., K.Y., and W. S. analyzed data, provided critical feedback and helped shape the research. X.Y., G.X., L.S., and P.H. wrote the manuscript with inputs from all co-authors.

DECLARATION OF INTERESTS

The authors declare no competing interests.

module in plant growth, development and immunity, *Arabidopsis thaliana* BRASSINOSTEROID INSENSITIVE 1-associated receptor kinase 1 (BAK1) and somatic embryogenesis receptor kinase 4 (SERK4) redundantly and negatively regulate plant cell death. By deploying an RNAi-based genetic screen for *bak1/serk4* cell death suppressors, we revealed that cyclic nucleotide-gated channel 20 (CNGC20) functions as a hyperpolarization-activated Ca^{2+}-permeable channel specifically regulating *bak1/serk4* cell death. BAK1 directly interacts with and phosphorylates CNGC20 at specific sites in the C-terminal cytosolic domain, which in turn regulates CNGC20 stability. CNGC19, the closest homolog of CNGC20 with a low abundance compared with CNGC20, makes a quantitative genetic contribution to *bak1/serk4* cell death only in the absence of CNGC20, supporting the biochemical data showing homo- and heteromeric assembly of the CNGC20 and CNGC19 channel complexes. Transcripts of *CNGC20* and *CNGC19* are elevated in *bak1/serk4* compared with wild-type plants, further substantiating a critical role of homeostasis of CNGC20 and CNGC19 in cell death control. Our studies not only uncover a unique regulation of ion channel stability by cell surface-resident receptor kinase-mediated phosphorylation, but also provide evidence for fine-tuning Ca^{2+} channel functions in maintaining cellular homeostasis by the formation of homo-and heterotetrameric complexes.

eTOC Summary:

Yu *et al.* show that BAK1/SERK4-mediated phosphorylation regulates Ca^{2+} channel CNGC20/CNGC19 stability for the precise control of plant cell death, revealing the critical function of CNGC20/CNGC19 in the regulation of cellular homeostasis for cell survival.

Keywords

Plant cell death; cyclic nucleotide-gated channel; Ca^{2+}-permeable channel; receptor kinase; cellular homeostasis; virus-induced gene silencing; phosphorylation

INTRODUCTION

Plants have evolved hundreds of cell surface-resident receptor-like kinases (RLKs) regulating plant growth, development, and defense [1, 2]. A large number of characterized RLKs contain an extracellular leucine-rich repeat (LRR) domain [1]. Several well-studied LRR-RLKs are *bona fide* receptors that perceive intrinsic and extrinsic factors derived from plant growth, development and environmental cues. These include FLAGELLIN-SENSING 2 (FLS2) perceiving bacterial flagellin in activating plant immune signaling, and BRASSINOSTEROID INSENSITIVE 1 (BRI1) perceiving plant growth hormone brassinosteroids (BRs) in regulating plant growth [3, 4]. BRI1-ASSOCIATED RECEPTOR KINASE 1 (BAK1), also known as SOMATIC EMBRYOGENESIS RECEPTOR KINASE 3 (SERK3), together with other SERKs, function as coreceptors of FLS2, BRI1 and some other LRR-RLKs, and regulate a wide range of physiological responses ranging from male gametophyte development, plant growth, stomatal patterning, to plant immunity [5–7].

A unique yet largely uncharacterized function of BAK1 and its closest homolog SERK4 is the containment of cell death [8, 9]. The *bak1/serk4* null mutant is postembryonic lethal associated with spontaneous cell death, constitutive H_2O_2 production, and pathogenesis-

related (*PR*) gene induction [9]. The *bak1–4/serk4–1* mutant shows severe seedling lethality and does not produce seeds preventing a classical suppressor screen. To understand the mechanisms underlying BAK1/SERK4-mediated cell death, we have designed a virus-induced gene silencing (VIGS), a type of RNA interference (RNAi), -based genetic screen for suppressors of *bak1/serk4* cell death using a sequence-indexed library of *Arabidopsis* T-DNA insertion lines [10]. Silencing of *BAK1* and *SERK4* by *Agrobacterium*-mediated VIGS in wild type (WT) Col-0 plants triggers cell death as observed in the *bak1–4/serk4–1* mutant. The screen has identified a series of mutants, including *stt3a*, which bears a mutation in the catalytic subunit of the oligosaccharyltransferase complex for protein *N*-glycosylation [10]. Members of cysteine-rich receptor-like kinases (CRKs), which are transcriptionally activated in *bak1/serk4*, are the client proteins of protein glycosylation regulating cell death process.

In this study, we report the involvement of cyclic nucleotide-gated channel 20 (CNGC20) and CNGC19 in regulating *bak1/serk4* cell death. The RNAi-based screen identified CNGC20, but not other CNGCs, as a specific regulator of *BAK1/SERK4* cell death. Although CNGC19 has no effect on its own, it contributes to *bak1/serk4* cell death in the absence of CNGC20. Consistent with this, both CNGC20 and CNGC19 are hyperpolarization-activated Ca^{2+}-permeable channels, and CNGC20 and CNGC19 have an additive effect on channel activity, suggesting that CNGC20 and CNGC19 form functional homo- and hetero-meric Ca^{2+} channels. BAK1 and SERK4 interact with and phosphorylate CNGC20, and likely CNGC19, which leads to the degradation of CNGC20 and CNGC19 proteins. In the *bak1/serk4* mutant, both CNGC20/CNGC19 protein and transcript levels are increased, leading to mis-regulation of Ca^{2+} influx and signaling, as a consequence, cellular homeostasis cannot be maintained and plants undergo cell death. Our studies reveal the critical function of CNGC20 and CNGC19 in the precise control of cellular homeostasis for cell survival, and elucidate the regulation of CNGC20/CNGC19 protein stability by BAK1/SERK4-mediated phosphorylation.

RESULTS

The *cngc20* mutants suppress *bak1/serk4* cell death

One mutant identified from VIGS-based genetic screen for suppressors of *bak1/serk4* cell death, which was named *bak to life 1* (*btl1*), is *SALK_013823C*. The *btl1* mutant suppressed the dwarfism and leaf chlorosis triggered by RNAi-*BAK1/SERK4* compared to WT plants (Figure 1A). Trypan blue staining confirmed that cell death was reduced in *btl1* (Figure S1A). Staining with 3,3′-diaminobenzidine (DAB) showed that the elevated H_2O_2 accumulation caused by RNAi-*BAK1/SERK4* was abolished in *btl1* (Figure S1B). Compared to WT, *btl1* showed reduced accumulation of *PR1* and *PR2* upon silencing of *BAK1*/*SERK4* (Figure S1C). Furthermore, *BTL1* specifically regulates *BAK1/SERK4*-mediated cell death and may not be involved in the cell death regulated by MEKK1, a MAP kinase (MAPK) kinase kinase downstream of BAK1/SERK4 in plant immunity [11], or BIR1, a BAK1-interacting LRR-RLK [12] (Figure S1D).

The *btl1* mutant (*SALK_013823C*) was annotated to bear a T-DNA insertion at the 8th intron of *AT1G60995* encoding an uncharacterized membralin domain-containing protein (Figure

S1E). However, neither two additional mutant alleles of *AT1G60995* (*SALK_087793C* and *SALK_042821C*) (Figure S1F–H), nor the complementation of *AT1G60995* under either the *35S* promoter or its native promoter (Figure S1I) supported that the annotated T-DNA insertion in *AT1G60995* was responsible for the suppression of RNAi-*BAK1/SERK4*-induced cell death in *btl1*. To identify the causal mutation, we performed whole genome-sequencing analysis and revealed that *btl1* carried two additional T-DNA insertions at *AT1G11020*, encoding a zinc finger superfamily protein, and *AT3G17700*, encoding CNGC20 (Figure S2A–C, Table S1 & S2). Neither mutant alleles of *AT1G11020* (*SALK_037558C* and *SAIL_302_A04*) suppressed RNAi-*BAK1/SERK4*-induced cell death (Figure S1J).

Importantly, two additional alleles, including *cngc20–1* (*SALK_129133C*) and *cngc20–2* (*SALK_074919C*) (Figure S2B, D & E), suppressed RNAi-*BAK1/SERK4*-induced cell death (Figure 1B). Resembling *btl1*, which was renamed as *cngc20–3*, the *cngc20–1* and *cngc20–2* mutants abolished cell death (Figure 1C), elevated H_2O_2 (Figure 1C) and accumulation of *PR1* and *PR2* genes (Figure 1D) caused by RNAi-*BAK1/SERK4*. Transformation of the *CNGC20* genomic fragment under the control of its native promoter into *cngc20–3* restored RNAi-*BAK1/SERK4*-induced cell death (Figure 1E). In addition, we generated the *bak1–4/serk4–1/cngc20–3* triple mutant by genetic crosses (Figure S2F). The *bak1–4/serk4–1/cngc20–3* mutant overcame seedling lethality of *bak1–4/serk4–1* and resembled WT plants at the two-week-old stage when grown on 1/2MS medium plates (Figure 1F). Cell death, H_2O_2 accumulation, and *PR1* and *PR2* expression were significantly ameliorated in *bak1–4/serk4–1/cngc20–3* compared to those in *bak1–4/serk4–1* (Figure 1G & H). When grown in soil, the *bak1–4/serk4–1/cngc20–3* mutant developed true leaves whereas *bak1–4/serk4–1* stopped development at the cotyledon stage (Figure 1F). Collectively, our genetic analyses demonstrate that the *CNGC20* mutation leads to the suppression of *bak1/serk4* cell death.

Specific function of CNGC20 in plant cell death control

The *Arabidopsis* genome encodes 20 *CNGC*s mediating abiotic and biotic stresses and developmental processes [13, 14]. To assess the involvement of additional CNGCs in *bak1/serk4* cell death, we systemically characterized all the available *cngc* mutants for suppression of RNAi-*BAK1/SERK4*-induced cell death (Figure 2A & Table S3). The *cngc18* mutant is male sterile and could not set homozygous seeds [15]. The *cngc2* and *cngc4* mutants, also known as *defense*, *no death 1* (*dnd1–1*) and *dnd2–1* respectively, are derived from ethyl methanesulfonate (EMS) mutagenesis and produce truncated proteins [16–18]. Genotyping and RT-PCR analyses of *cngc1, 3, 5, 6, 7, 8, 9, 10, 11, 12, 13, 14, 15, 16, 17* and *19* mutants confirmed that all these mutants, except *cngc7* showing a WT genotyping, are homozygous for the T-DNA insertion and showed reduced *CNGC* transcripts accordingly (Figure S3A & B). However, none of these *cngc* mutants, including *cngc19*, the gene of which is the closest homolog of *CNGC20*, suppressed RNAi-*BAK1/SERK4*-induced cell death (Figure 2A), indicating a specific function of *CNGC20* in *bak1/serk4* cell death.

CNGC20 and CNGC19 belong to group IV of *Arabidopsis* CNGCs together with CNGC2 and CNGC4, which have been shown to regulate plant immunity [16–21]. CNGC19, not CNGC20, has been recently shown to regulate *Arabidopsis* defense against Spodoptera herbivory [22]. Plants have developed a two-tiered immune system: effector-triggered immunity (ETI) and microbe/danger-associated molecular pattern (MAMP/DAMP)-triggered immunity (PTI) to ward off pathogen invasions [23–25]. CNGC11 and CNGC12 are involved in plant ETI [26]. We assessed the involvement of CNGC20 in plant ETI and/or PTI. The *cngc20* mutants showed similar pathogen resistance as WT, as shown in bacterial growth and symptom development to *Pseudomonas syringae* pv. *tomato* (*Pst*) DC3000 carrying *avrRpt2* (Figure S4A) or *avrRps4* (Figure S4B). ETI is often associated with localized cell death, referred as the hypersensitive response (HR). The progression of *Pst avrRpt2*- or *Pst avrRpm1*-triggered HR was similar in the *cngc20* mutants as that in WT plants (Figure S4C & D). In addition, the *cngc20* mutants did not affect plant resistance to the virulent *P. syringae* pv. *maculicola* (*Psm*) ES4326 in terms of bacterial growth and disease symptom development (Figure S4E). Furthermore, the *cngc20* mutants did not affect MAMP flg22-, a 22-amino acid synthetic peptide corresponding to bacterial flagellin, or DAMP Pep1-induced early PTI signaling events such as ROS production, MAPK activation, and receptor-like cytoplasmic kinase (RLCK) BIK1 phosphorylation (Figure 2B–E). These data suggest that unlike CNGC2, 4, 11 and 12, CNGC20 is not involved in plant ETI and PTI.

BAK1, the shared co-receptor of multiple LRR-RLKs, positively regulates plant immunity and development [5, 6]. The *bak1* mutant is compromised in flg22-triggered immunity and BR-mediated development with rounder leaves and shorter petioles. Since the mutation in *cngc20* suppressed *bak1/serk4* cell death, we tested whether *cngc20* interferes with the *bak1–4* deficiency in plant immunity and growth using the *bak1–4/cngc20–1* double mutant. The compromised flg22-induced MAPK activation and BIK1 phosphorylation remained similar in *bak1–4/cngc20–1* as those in *bak1–4* (Figure 2D & E). Similar to *bak1–4, bak1–4/cngc20–1* showed compromised expression of flg22-induced genes, *WRKY30* and *MYB15*, compared with WT or *cngc20–1* (Figure 2F). In addition, the *cngc20–1/bak1–4* mutant resembles *bak1–4* in its growth morphology (Figure 2G). Collectively, the evidence suggests a specific involvement of *CNGC20* in *BAK1/SERK4*-mediated cell death containment, uncoupled from *BAK1/SERK4* functions in plant immunity and growth.

BAK1 interacts with and phosphorylates CNGC20

Both CNGC20 and BAK1 exhibit plasma membrane-localization [27, 28]. We examined whether CNGC20 associates with BAK1. A co-immunoprecipitation (Co-IP) assay from co-expression of FLAG-tagged CNGC20 and HA-tagged BAK1 in *Arabidopsis* protoplasts indicated that BAK1 co-immunoprecipitated CNGC20 (Figure S5A). When transiently expressed in *Nicotiana benthamiana*, BAK1-FLAG immunoprecipitated CNGC20-HA (Figure S5B). We further transformed *pCNGC20::CNGC20-HA* into *pBAK1::BAK1-FLAG* transgenic plants. BAK1 immunoprecipitated CNGC20 when both were expressed under their native promoters, indicating that BAK1 associates with CNGC20 *in vivo* (Figure 3A). The association between BAK1 and CNGC20 at the plasma membrane was confirmed by a bimolecular fluorescence complementation (BiFC) assay (Figure 3B). The observed puncta

of BAK1-nYFP and CNGC20-cYFP close to plasma membrane suggest that they may also localize to endosomal compartments [28]. CNGC20 is a transmembrane protein consisting of N-terminal and C-terminal cytosolic domains (CNGC20N and CNGC20C) and six transmembrane domains (Figure 3C). The BAK1 cytosolic domain ($BAK1^{CD}$), including juxtamembrane and kinase domains, immunoprecipitated both CNGC20N and CNGC20C (Figure S5C). We further tested whether CNGC20N or CNGC20C directly interacted with BAK1 in an *in vitro* pull-down assay. The maltose-binding protein (MBP)-tagged $BAK1^{CD}$ (MBP-$BAK1^{CD}$) was pulled down by glutathione S-transferase (GST)-tagged CNGC20N or CNGC20C but not GST itself (Figure 3D & E). Moreover, the interaction between the BAK1 kinase domain ($BAK1^{K}$) and CNGC20N was confirmed by a yeast two-hybrid assay (Figure 3F). Interestingly, the BAK1 kinase inactive mutant ($BAK1^{CD}KM$) showed a reduced interaction with CNGC20C, indicating a requirement of BAK1 kinase activity for a full interaction (Figure S5D). Together, the data elucidate that CNGC20 interacts with BAK1 via its N- and C-terminal cytosolic domains.

We next tested whether BAK1 could phosphorylate CNGC20. An *in vitro* kinase assay indicated that $BAK1^{CD}$, but not $BAK1^{CD}KM$, directly phosphorylated both CNGC20N and CNGC20C (Figure S5E & F). The $BAK1^{CD}$-phosphorylated CNGC20N and CNGC20C proteins were subjected to trypsin digestion and liquid chromatography-tandem mass spectrometry (LC-MS/MS) analysis. We identified Ser^{184} as a confident and Ser^{156} as a less confident $BAK1^{CD}$ phosphorylation site on CNGC20N (Figure S6A), and multiple confident $BAK1^{CD}$ phosphorylation sites on CNGC20C, including Thr^{560}, Ser^{617}, and Ser^{618} (Figure 4A, B, S6B & C). In addition, Thr^{619} was identified as a potential phosphorylation site on CNGC20C (Figure 4A). Both Ser^{156} and Ser^{184} have potential phosphorylatable residues next to them, Thr^{155} and Ser^{185} on CNGC20N. We mutated all four of these residues on CNGC20N to Ala, and the $Thr^{155A}Ser^{156A}Ser^{184A}Ser^{185A}$ quadruple mutant ($CNGC20N^{QA}$) did not affect the phosphorylation by BAK1 (Figure 4C). CNGC20C Thr^{560A} also did not affect the phosphorylation by BAK1 (Figure S6D). However, the $Thr^{560A}Ser^{617A}Ser^{618A}Thr^{619A}$ quadruple mutant ($CNGC20C^{QA}$) of CNGC20C compromised its phosphorylation by BAK1 (Figure 4D), implying an important role for CNGC20 C-terminal phosphorylation by BAK1. These phosphorylation sites locate to the C-linker and cyclic nucleotide-binding domain (CNBD) (Figure 4E & S6E). This re-elaborates a postulated regulatory role of the C-terminus for CNGC functions. For example, several residues in the C-terminus of human hyperpolarization-activated cyclic nucleotide-gated (HCN) channels and *Arabidopsis* CNGC11/CNGC12 are critical for inter-subunit interactions [29, 30].

BAK1 regulates CNGC20 stability

Since loss of *CNGC20* suppressed *bak1/serk4* cell death and BAK1 phosphorylates CNGC20, it is tempting to speculate that abundance and/or activity of CNGC20 is regulated by BAK1-mediated phosphorylation. Notably, the *Lotus japonicus* CNGC20 homolog makes a quantitative contribution to root development and infection by nitrogen-fixing rhizobia and its expression level is a key for its function [31]. In addition to tissue expression specificity, transcript levels of some *CNGCs* are regulated upon pathogen infections [32]. We observed an elevated level (about 4–6 fold) of *CNGC20* and *CNGC19* transcripts in *bak1–4/serk4–1*

compared with WT (Figure 5A) based on RNA-Seq analysis [10]. When expressed under the control of the *35S* promoter, the protein expression level of CNGC20-HA in *bak1–4* was much higher than that in WT (Figure 5B). These data indicate that both CNGC20 transcripts and proteins are regulated by BAK1 and SERK4. Conversely, when co-expressing BAK1 or SERK4 with CNGC20 in *Arabidopsis* protoplasts, the protein level of CNGC20, but not the GFP control, was reduced (Figure 5C & S6F). The CNGC20 protein level was higher when coexpressed with the BAK1 kinase inactivate mutant than that with WT BAK1 (Figure 5D), implying the importance of BAK1 phosphorylation on CNGC20 abundance. Similarly, the kinase inhibitor K252a increased the protein level of CNGC20-HA (Figure 5E). Further, pretreatment with MG132, a protein degradation inhibitor, increased CNGC20 protein accumulation when transiently expressed in *N. benthamiana* (Figure 5F) or in the *pCNGC20::gCNGC20-HA*/*cngc20* transgenic plants (Figure 5G). Therefore, the stability of CNGC20 proteins is likely regulated by BAK1 phosphorylation.

To elucidate the role of BAK1 phosphorylation on CNGC20, we generated the phosphomimetic form of CNGC20 ($CNGC20^{QD}$), in which four critical phosphorylation sites (Thr^{560}/Ser^{617}/Ser^{618}/Thr^{619}) in CNGC20C were mutated to Asp, and transformed into *cngc20–1*. Unlike CNGC20, $CNGC20^{QD}$ did not restore cell death, H_2O_2 accumulation and *PR* gene expression caused by silencing of *BAK1/SERK4* (Figure 5H, 5I & S6G), suggesting that BAK1 phosphorylation of CNGC20 at Thr^{560}/Ser^{617}/Ser^{618}/Thr^{619} suppresses *bak1/serk4* cell death. Consistent with the notion that BAK1 phosphorylation negatively regulates CNGC20 protein stability, the $CNGC20^{QD}$-HA protein level was substantially lower than CNGC20-HA and barely detectable in the *pCNGC20::gCNGC20^{QD}-HA* complementation lines compared with the *pCNGC20::gCNGC20-HA* plants (Figure 5J). Notably, the reduced abundance of $CNGC20^{QD}$-HA proteins was not due to the reduction of *CNGC20* transcripts (Figure 5J). Thus, the data suggest that BAK1-mediated phosphorylation at Thr^{560}/Ser^{617}/Ser^{618}/Thr^{619} negatively regulates CNGC20 abundance and the homeostasis of CNGC20 is vital in *bak1/serk4* cell death.

CNGC19 and CNGC20 are hyperpolarization-activated Ca^{2+} permeable channels

CNGCs function as non-selective cation channels. Evidence from electrophysiological and physiological studies supports that plant CNGCs are inward rectifying Ca^{2+} channels [21, 31, 33]. To determine whether CNGC20 possesses permeability to Ca^{2+}, we injected *YFP-CNGC20* capped RNAs into *Xenopus* oocytes for two-electrode voltage clamping (Figure 6A). Oocytes expressing YFP-CNGC20, but not the water-injected controls, exhibited significant inward currents at negative voltages in the presence of 10 or 30 mM Ca^{2+} (Figure 6B), indicating CNGC20 possesses Ca^{2+} channel activity. The CNGC20 channel activity appeared higher with 30 mM Ca^{2+} than that with 10 mM Ca^{2+} (Figure 6B), suggesting a Ca^{2+} dose-dependent activity. Of 20 CNGCs in *Arabidopsis*, CNGC19 and CNGC20 share the highest homology and are tandemly located on Chromosome 3 [13, 14]. Expression of YFP-CNGC19 in *Xenopus* oocytes also led to a Ca^{2+} dose-dependent channel activity (Figure 6A & C). Apparently, when CNGC19 and CNGC20 were co-expressed together in *Xenopus* oocytes, the channel activity was increased compared to CNGC19 or CNGC20 alone (Figure 6A & D). Likewise, when expressed in the yeast mutant strain K927

(cchl::TRP1), which shows a lethality phenotype upon treatment with α-mating factor due to the lack of the CCH1 Ca^{2+} channel [34], CNGC20 or CNGC19 alone weakly, but significantly, complemented the phenotype while the combination of CNGC20 and CNGC19 showed a strong complementation (Figure 6E). These results suggest that both CNGC19 and CNGC20 confer hyperpolarization-activated Ca^{2+} permeable channel activity. Ca^{2+} is an essential second messenger in nearly every aspect of cellular signaling programs [35]. Therefore, we speculate that mis-regulation of Ca^{2+} influx through CNGCs in *bak1/serk4* leads to the uncontrolled activation of downstream signaling events, contributing to cell death, ROS production and defense gene induction.

CNGC19 contributes to *bak1/serk4* cell death in the absence of CNGC20 and dimerizes with CNGC20

Although the *cngc19* single mutant did not affect *bak1/serk4* cell death, the additive effects of CNGC19 and CNGC20 in channel activity and complementing yeast mutant growth (Figure 6D & E) prompted us to test whether CNGC19 and CNGC20 additively regulate *bak1/serk4* cell death. We generated the *bak1–4/serk4–1/cngc20–1/cngc19* quadruple mutants using CRISPR/Cas9 genome editing to introduce lesions in *CNGC19* in the *bak1–4/serk4–1/cngc20–1* background. The homozygous *bak1–4/serk4–1/cngc20–1/cngc19* quadruple mutants contain an adenine insertion in the fourth exon of *CNGC19*, which caused a frameshift mutation leading to a premature stop codon (Figure 7A & S7A). When grown on soil, the *bak1/serk4/cngc20* mutant showed the growth retardation three weeks after germination and could not set seeds at 23°C (Figure 1F). However, the *bak1/serk4/cncg19/cngc20* quadruple mutants almost fully rescued the cell death phenotype of *bak1/serk4* and were able to set seeds normally (Figure 7A). Thus, CNGC19 makes undetectable contributions to *bak1/serk4* cell death in the presence of CNGC20, however, it contributes to *bak1/serk4* cell death when CNGC20 is absent. Notably, the *CNGC20* transcripts were about ~10 fold higher than *CNGC19* in WT plants (Figure 5A), reinforcing the primary role of CNGC20 in regulating *bak1/serk4* cell death. Taken together, CNGC20 plays a major role with a quantitative effect of CNGC19 in regulating *bak1/serk4* cell death.

Conventional animal CNGC channels exist as heterotetramers composed of A and B subunits [29]. Plant CNGCs also form both homomeric and heteromeric tetramers [15, 36]. To examine whether CNGC19 and CNGC20 also assemble a multi-unit protein complex, we tested the association between CNGC19 and CNGC20 with BiFC and Co-IP assays. CNGC20 associated with CNGC19 in *Arabidopsis* protoplasts (Figure 7B & C). In addition, both CNGC20 and CNGC19 were self-associated, suggesting that CNGC20 and CNGC19 likely function as homo- and heteromeric protein complexes (Figure 7C). Human CNGCs assemble via the C-terminal cytosolic domain [29]. Similarly, CNGC20C self-associated in *Arabidopsis* protoplasts (Figure S7B). Similar to CNGC20, CNGC19 also associated with BAK1 (Figure 7B & D). The four critical BAK1 phosphorylation sites (Thr^{560}/Ser^{617}/Ser^{618}/Thr^{619}) in CNGC20 are all conserved in CNGC19 (Figure S6E). In accordance, the CNGC19 protein level was regulated by BAK1/SERK4 (Figure 7E), likely through phosphorylation on those conserved sites. Thus, the data indicate functional homo- and heteromeric channel complexes of CNGC20 and CNGC19 regulated by BAK1 and SERK4.

The additive function of CNGC19 and CNGC20 in *bak1/serk4* cell death led us to examine whether they regulate immune signaling in a similar manner. The *cngc19/cngc20* double mutants were generated by introducing the same CRISPR/Cas9 *CNGC19* construct into *cngc20–1*. flg22-induced MAPK activation remained similar to WT in two independent *cngc19/cngc20* lines (Figure S7C). The *cngc19/cngc20* mutant also did not affect flg22-induced Ca^{2+} influx, another early PTI event, which was measured by the single-wavelength fluorescent Ca^{2+} indicator GCaMP3 (Figure S7D). Neither *cngc20* nor *cngc19/cngc20* affected Pep1-mediated seedling growth inhibition (Figure S7E). Additionally, disease resistance to *Pst* DC3000 or *Pst* DC3000 *avrRpt2* in *cngc19/cngc20* plants was similar to that of WT (Figure S7F & G). Therefore, CNGC19 and CNGC20 are unlikely involved in plant PTI and ETI.

DISCUSSION

As a shared coreceptor, BAK1 interacts with and trans-phosphorylates cognate receptors [5, 6]. Few BAK1 substrates in transducing intracellular signaling have been identified. We show here that BAK1 directly interacts with and phosphorylates a functional Ca^{2+}-permeable channel CNGC20, and likely CNGC19, at C-terminal specific sites (Figure 7F). The C-terminal cytosolic domain of mammalian CNGCs has been recognized to be essential for subunit interactions and cyclic nucleotide gating [29]. Intriguingly, BAK1-mediated phosphorylation regulates CNGC20 and CNGC19 stability and homeostasis. Although the regulatory mechanism remains unclear, BAK1 also interacts with CNGC17, which may form a functional cation-translocating unit with H^+-ATPases for Phytosulfokine (PSK) receptor-mediated root growth [37]. Additionally, BAK1 phosphorylates sugar transport protein 13 (STP13) to enhance its monosaccharide uptake activity, thereby competing with bacteria for extracellular sugars likely as a defense mechanism [38]. Apparently, in addition to signaling molecules, ion channels and transporters are also regulated by cell surface-resident RLKs for their homeostasis and activation.

Two recent reports show that plant RLCKs phosphorylate and activate CNGCs mediating MAMP-induced Ca^{2+} influx in plant PTI [21, 33]. *Arabidopsis* RLCK BIK1 interacts and activates CNGC2 and CNGC4 by phosphorylation, leading to an increase of cytosolic Ca^{2+} [21]. Rice OsRLCK185 directly interacts and phosphorylates OsCNGC9 to activate its channel activity and regulate rice resistance to blast disease [33]. Notably, phosphorylation by BIK1, a direct substrate of BAK1 [39], contributes to the activation of CNGC2/CNGC4 channel activity in PTI signaling, whereas phosphorylation by BAK1 diminishes CNGC19/CNGC20-mediated signaling in controlling cell survival. In addition, CNGC2 and CNGC4 likely assemble into a functional heterotetrameric Ca^{2+} channel and neither CNGC2 nor CNGC4 alone is a functional channel [21], which is different from that CNGC20 and CNGC19 form functional homo- and hetero-meric Ca^{2+} channels. These parallel but distinct regulatory mechanisms further emphasize the importance of BAK1 in bifurcating the signaling specificity of various biological processes, as well as the diverse functions and regulations of CNGC family proteins.

It has been shown previously that protein glycosylation is involved in regulating *bak1/serk4* cell death [10]. There are six and eight potential glycosylation sites in CNGC20 and

CNGC19 respectively. It will be interesting to test in the future whether CNGC19/CNGC20 are glycosylated and whether glycosylation is important for their function. In addition, cytoplasmic export of mRNAs plays a role in *bak1/serk4* cell death [40]. It is possible that the nucleocytoplasmic trafficking facilitates the export of *CNGC20* and *CNGC19* transcripts from nucleus, which further contributes to the cell death in *bak1/serk4*. Alternatively, it has been hypothesized that BAK1/SERK4 may play a role in keeping in check the specific cellular perturbation and safeguarding cellular homeostasis for cell survival [8]. This notion is supported by our current results that BAK1/SERK4 keep CNGC19/CNGC20 proteins at a low level under normal growth conditions. When this regulation is absent (i.e. in the *bak1/serk4* mutant,) cellular homeostasis or cell survival cannot be maintained, thus, as a consequence, the cell undergoes cell death. In summary, our results pinpoint a regulatory mechanism where the homeostasis of CNGC20 and CNGC19 modulated by receptor-like kinase BAK1-mediated phosphorylation is the key for precise control of plant cell death, which expands the portfolio of CNGC functions and regulations.

STAR METHODS

LEAD CONTACT AND MATERIALS AVAILABILITY

Further information and requests for resources should be directed to and will be fulfilled by the Lead Contact, Libo Shan (lshan@tamu.edu). we will distribute the plasmids and transgenic plants freely to the scientific community upon request.

EXPERIMENTAL MODEL AND SUBJECT DETAILS

***Arabidopsis thaliana* and growth conditions—**All *Arabidopsis* plants used in this study were in the Columbia-0 (Col-0) background. The various mutants and transgenic lines used in this study were described in the Key Resources Table. *Arabidopsis* lines were grown in soil (Metro Mix 366) in a growth room at 23°C, 45% humidity and 85μE $m^{-2}s^{-1}$ light with a 12-hr light/12-hr dark photoperiod for two-weeks before VIGS assays or 30 days for protoplast isolation, ROS production and pathogen assays. Seedlings were germinated on plates containing half-strength Murashige and Skoog medium (1/2MS) with 0.5% sucrose, 0.8% agar and 2.5 mM MES at pH 5.7, and grown under the same growth condition as above for 10 days. The seedlings were transferred to a 6-well tissue culture plate with 2 ml H_2O for overnight, and then used for indicated assays.

Nicotiana benthamiana* and growth conditions—Nicotiana benthamiana* was grown in greenhouses in soil under a 12-hr light/12-hr dark photoperiod at 23°C.

Bacterial strains—The various bacteria strains used in this study were described in the Key Resources Table. *Pseudomonas syringae* pv. tomato (*Pst*) DC3000 were grown on the King's B medium plates with 50 μg/ml rifampicin. *Pst* DC3000 carrying *avrRpt2*, *avrRps4* or *avrRpm1* was grown with 50 μg/ml kanamycin and 50 μg/ml rifampicin [41–43]. *P. syringae* pv. *maculicola* ES4326 (*Psm*) was grown with 50 μg/ml Streptomycin [44]. All the *Pseudomonas* strains were grown on plates at 28°C for 2 days for further inoculum preparation.

METHOD DETAILS

Plasmid construction and generation of transgenic plants—The VIGS of *BAK1/SERK4, MEKK1* and *BIR1* constructs and the *pHBT-BIK1-HA*, *pHBT-BAK1-HA, pHBT-BAK1-FLAG, pMAL-BAK1^{CD}-HA*, and *pMAL-BAK1^{CD}KM-HA* constructs were reported previously [10, 45]. The *CNGC19* and *CNGC20* genes were amplified from Col-0 cDNA with primers containing NcoI at N-terminus and StuI at C-terminus (Supplemental Table S4), and ligated into a plant protoplast expression vector *pHBT* under the control of a CaMV *35S* promoter with an *HA*, *FLAG*, *cYFP* or *nYFP* tag at C-terminus. N-terminus and C-terminus of *CNGC20* (*CNGC20N* and *CNGC20C*) were cloned using the above constructs as the templates and primers as listed in the Supplemental Table S4. The point mutations of *CNGC20N$^{T145/S146/S183/S184A}$*, *CNGC20C^{T560A}*, *CNGC20C$^{T560/S617/S618/T619A}$*, *CNGC20$^{T560/S617/S618/T619D}$* were generated by site-directed mutagenesis with primers listed in Supplemental Table S4. To construct the *E.coli* expression vectors, *CNGC20N*, *CNGC20C*, *CNGC20N$^{T145/S146/S183/S184A}$*, *CNGC20C^{T560A}* and *CNGC20C$^{T560/S617/S618/T619A}$* were subcloned into a modified GST fusion protein expression vector pGEX4T-1 (Pharmacia) using BamHI (the enzyme site located in front of NcoI on the *pHBT* vector) and StuI digestion. The *CNGC20N* was subcloned into a modified pGBKT7 vector (Clontech) for yeast two-hybrid assays using BamHI and StuI digestion. To introduce *CNGC20* into the binary vectors, the *CNGC20* fragment was released from the *pHBT* vector using BamHI and StuI digestion and ligated into the *pCB302* (*35S* promoter) or *pMDC* (*2×35S* promoter) binary vectors.

To construct the *pCAMBIA1300* binary vector containing the native promoter driven g*CNGC20* for *Agrobacterium*-mediated transformation, the genomic fragment of the *CNGC20* gene (*gCNGC20*) was amplified from Col-0 genomic DNA using primers containing NcoI at N-terminus and StuI at C-terminus (Supplemental Table S4), and ligated into *pHBT* under the control of the *35S* promoter with an HA epitope-tag at its C-terminus to obtain the *pHBT-p35S::gCNGC20-HA* vector. The *CNGC20* promoter (2 kb upstream of the start codon) was amplified from Col-0 genomic DNA using primers containing XhoI at N-terminus and NcoI at C-terminus (Supplemental Table S4), and ligated into *pHBT-p35S::gCNGC20-HA* to obtain the *pHBT-pCNGC20::gCNGC20-HA* vector. The native promoter driven *gCNGC20* together with the *HA* epitope and the *NOS* terminator were released from *pHBT-pCNGC20::gCNGC20-HA* using XhoI/EcoRI digestion and ligated into *pCAMBIA1300* to obtain the *pCAMBIA1300-pCNGC20::gCNGC20-HA* binary vector. The point mutations of *gCNGC20$^{T560/S617/S618/T619D}$* were generated by site-directed mutagenesis in the corresponding vector.

To construct the oocyte expression vectors for electrophysiology studies, *CNGC19* and *CNGC20* were cloned into the *pNB1* serial vectors using the USER method to obtain *pNB1YFP-CNGC19*, *pNB1YFP-CNGC20*, *pNB1YC-CNGC19* and *pNB1YN-CNGC20* expression vectors [46]. Uracil-containing forward primer was designed as 5’-GGCTTAAU + sequence complementary to the target gene-3’, and reverse primer as 5’-GGTTTAAU + sequence complementary to the target gene-3’. PCR was performed with Phusion U Hot Start DNA polymerase (Thermo Fisher, F555) according to manufacturer’s instruction. The reaction mixture containing PCR product, USER enzyme mix (New England Biolabs,

M550), and PacI/Nt.BbvCI digested *pNB1* vector was incubated 20 min at 37°C followed by 20 min at 25°C, and then transformed into chemically competent *E. coli* cells. PCR and Sanger sequencing were performed to confirm the positive clones.

To construct the CRISPR/Cas9 *CNGC19* vector, two suitable guide RNAs (gRNAs) without predicted off-targets were designed via the website http://chopchop.cbu.uib.no/. gRNA1, located in the 4th exon of *CNGC19* (5'-GAGTCTAGAATAGTTGGTGC-3'), and gRNA2, located in the 5th exon of *CNGC19* (5'-CGAAGTCACAACGAGATCTG-3'), were incorporated into the gRNA expression cassette by the first round PCR using *pCBC-DT1T2* [47] as a template. The resulting PCR fragments were further used as the template to incorporate the BsaI restriction enzyme site through the second round PCR. The final PCR fragments were inserted into the BsaI site of the CRISPR/Cas9 *pHEE401E* vector [47].

The *AT1G60995* gene was amplified from Col-0 cDNA with primers containing XbaI and NcoI at N-terminus and StuI at C-terminus (Supplemental Table S4), and ligated into the binary vector *pCB302* under the control of the *35S* promoter with an HA tag at C-terminus to generate *pCB302-p35S::AT1G60995-HA*. The promoter of *AT1G60995* (520 bp upstream of the start codon) was amplified from Col-0 genomic DNA using primers containing SacI at N-terminus and XbaI at C-terminus (Supplemental Table S4), and ligated into *pCB302-p35S::AT1G60995-HA* to generate *pCB302-pAT1G60995::AT1G60995-HA* vector.

The promoter of *BAK1* (1.5kb upstream of the start codon) was amplified from Col-0 genomic DNA using primers containing XhoI and XbaI at N-terminus and BamHI at C-terminus (Supplemental Table S4), and ligated into *pHBT-p35S::BAK1-FLAG* to obtain *pHBT-pBAK1::BAK1-FLAG*. The native promoter driven *BAK1* was released using XbaI/StuI digestion and ligated into *pCB302* with a FLAG tag at the C terminus to obtain the *pCB302-pBAK1::BAK1-FLAG* binary vector.

The sequences of all genes, promoters or gRNAs were verified by the Sanger-sequencing. These binary plasmids were transformed into *Agrobacterium tumefaciens* strain GV3101 and then introduced into *Arabidopsis* using the floral dipping method.

Agrobacterium-mediated floral dipping—*Agrobacterium tumefaciens* GV3101 containing the binary vector was cultured at 28°C in LB liquid medium with 50 μg/ml Kanamycin and 25 μg/ml Gentamicin. Bacteria were harvested by centrifugation at 3000 rpm for 15 min and the pellet was suspended with buffer containing 50 mM MES (pH 5.5–5.7), 5% sucrose and 200 μl/L silwetL-77 at the density of OD_{600} =0.8. *Arabidopsis* flower buds were dipped thoroughly to the bacteria solution and then the dipped plants were covered with a dome for 24 hr to maintain high humidity. After that, plants were placed in the greenhouses under 12-hr light/12-hr dark light period and seeds were harvested for transgenic plants selection.

Elicitor and chemical inhibitor treatments—The elicitors flg22 and Pep1 were reported previously [48]. MG132 (AG Scientific #99533-80-9) and K252a (AG Scientific #133407-82-6) were diluted from DMSO stock solutions (2 mM for MG132 and 2 mM for K252a).

Trypan blue and DAB staining—Trypan blue staining and 3, 3′-diaminobenzidine (DAB) staining were performed according to procedures described previously with modifications. Briefly, the excised plant leaves were immersed in trypan blue staining solution (2.5 mg/mL trypan blue in lactophenol [lactic acid: glycerol: liquid phenol: H_2O = 1:1:1:1]) or DAB solution (1 mg/mL DAB in 10 mM Na_2HPO_4 and 0.05% Tween 20). Samples were vacuum-infiltrated for 30 min and then incubated for 8 hr at 25°C with gentle shaking at 75 rpm. Subsequently, samples were transferred to trypan blue destaining solution (ethanol: lactophenol = 2:1) or DAB destaining solution (ethanol: acetic acid: glycerol = 3:1:1) and incubated at 65°C for 30 min. The samples were then incubated in fresh destaining solution at room temperature until complete destaining. Pictures were taken under a dissecting microscope with samples in 10% glycerol.

***Agrobacterium*-mediated virus-induced gene silencing (VIGS) assay—**Plasmids containing binary TRV vectors *pTRV-RNA1* and *pTRV-RNA2* derivatives, *pYL156-BAK1/SERK4, pYL156-MEKK1, pYL156-BIR1, pYL156-GFP* (the vector control) were introduced into *Agrobacterium tumefaciens* strain GV3101 by electroporation. Bacterial cultures were first grown in LB medium containing 50 μg/ml kanamycin and 25 μg/ml gentamicin for overnight and then sub-cultured in fresh LB medium containing 50 μg/ml kanamycin and 25 μg/ml gentamicin supplemented with 10 mM MES and 20 μM acetosyringone for overnight at 28°C in a roller drum. Cells were pelleted by 4200 rpm centrifugation, re-suspended in a solution containing 10 mM $MgCl_2$, 10 mM MES and 200 μM acetosyringone, adjusted to OD_{600} of 1.5 and incubated at 25°C for at least 3 hr. Bacterial cultures containing *pTRV-RNA1* and *pTRV-RNA2* derivatives were mixed at a 1:1 ratio and inoculated into the first pair of true leaves of two-week-old soil-grown plants using a needleless syringe.

Electrophysiological Studies in *Xenopus laevis* Oocytes—Capped RNAs (cRNAs) were *in vitro* transcribed from the linearized *pNB1* vectors using the mMESSAGE mMACHINE T7 high yield RNA Transcription Kit following the manufacturer's protocol (Ambion). The quality of cRNAs was checked by Nanodrop and concentration was adjusted to the same level and stored at −80°C until injection. The expression and Two-Electrode Voltage-Clamp Recordings *Xenopus* oocytes were performed as described previously [49]. *Xenopus* oocytes were harvested at the stage V to VI and kept in a ND96 perfusion solution (96 mM NaCl, 2 mM KCl, 1 mM $CaCl_2$, 1 mM $MgCl_2$, 5 mM HEPES, 10 mM sorbitol, pH was adjusted to 7.4 with NaOH) for overnight prior to injections. Each oocyte was injected with 25 ng cRNAs or the same amount of water. Injected oocytes were incubated in perfusion solution at 18 °C for two days, and the protein expression was detected by YFP fluorescence signals (excited at 514 nm) using the Leica SP8 Laser confocal microscope. The currents were recorded with hyperpolarized pulses of a 0.1-s pre-pulse at −40 mV, followed by voltage steps of 0 to −180 mV (step at −20 mV, 1.5-s duration) and a 0.5-s deactivation at −40 mV using Axon Axoclamp 900A Microelectrode Amplifier. The bath solution for current recording contained 10 mM or 30 mM $CaCl_2$, 10 mM MES-Tris pH7.4, and osmolality was adjusted to 220 mOsm/L with mannitol. The pipette solution contained 3 M KCl.

Analysis of mutations at CRISPR-Cas9 target sites—Genomic DNAs were extracted from individual CRISPR/Cas9 transgenic T1 plants and WT plants. About 1100-bp fragments covering the targeted locus of the gRNAs were amplified by PCR using primers *gCNGC19*-CRISPR listed in Supplemental Table S4 and subjected for enzyme digestions. NlaIV was used to detect the mutation in the first target site and BglII was used for the second target site. Sanger sequencing of the PCR products using both the forward and reverse primers of *gCNGC19*-CRISPR was performed to verify the presence of mutations. Transgenic plants carrying mutations, especially in the gRNA1 target locus, were kept to harvest seeds. PCR products obtained using DNAs from individual T_2 plants were analyzed by enzyme digestion and Sanger sequencing as mentioned above to confirm the mutations in T_2 plants, and T_3 homozygous mutants carrying mutation in the gRNA1 target locus were kept for seeds.

Next generation sequence analysis of *cngc20–3* (*SALK_013823C*) to map T-DNA insertions—The genomic DNAs of *cngc20–3* were isolated for 100 nt paired-end sequencing on an Illumina HiSeq 2000 platform at Texas AgriLife Genomics and Bioinformatics Service (TAGS) (College Station, TX, USA). The Illumina reads of *cngc20–3* were first aligned to TAIR10 release of the Col-0 genome using the Bowtie aligner software with no more than three mis-matches [50]. A total of 9,527,475 (account for 90.6%) reads have been aligned. The unaligned reads were recovered and mapped to the T-DNA vector (pROK2) sequence with no more than three mismatches, and 2,182 reads have been mapped. The remaining unaligned reads (988,418), which were neither aligned to the Col-0 genome sequence nor the T-DNA vector sequence, were of interest to map over the T-DNA insertion breakpoint and reveal their locations. These reads were first blasted against the T-DNA vector sequence to retrieve any reads hitting to the T-DNA vector sequence and then blasted against the Col-0 genome sequence. In total, 20 reads aligned to both the T-DNA boarder sequence and the Col-0 genome sequence were retrieved and verified by the CLC Genomics Workbench 6.0.1 software (http://www.clcbio.com). Three major breakpoints in *AT1G60995, AT1G11020* and *AT3G17700* (*CNGC20*) were detected and confirmed by Sanger-sequencing using primers upstream and downstream of each breakpoint.

RT-PCR and qRT-PCR analysis—Total RNA was isolated from ten-day-old seedlings grown on 1/2MS plates or leaves of soil-grown plants two weeks after *Agrobacterial* inoculation for VIGS assay with TRIzol reagent. RNA was reverse transcribed to synthesize first strand cDNA with M-MuLV reverse transcriptase and oligo (dT) primer following RNase-free DNase I treatment. RT-PCR analysis was carried out using Taq DNA polymerase. Fragments of target genes were amplified using the primers listed in Table S4. *UBQ1* or *ACTIN2* was used as an internal control. Fragments were separated in 1.5% agarose gel and revealed by ethidium bromide staining and UV light exposure. Quantitative RT-PCR (qRT-PCR) analysis was carried out using iTaq SYBR green Supermix supplemented with ROX in an ABI GeneAmp® PCR System 9700. The expression of genes was normalized to the expression of *UBQ10* or *ACTIN2*.

MAPK assay—Ten-day-old seedlings grown on 1/2MS plates were transferred to water for overnight-recovery and then treated with 100 nM flg22 for indicated times. Each sample containing three seedlings was grounded in 40 ul of extraction buffer (150 mM NaCl, 50 mM Tris-HCl pH 7.5, 5 mM EDTA, 1% Triton X-100, 1 mM Na_3VO_4, 1 mM NaF, 1 mM DTT, 1:200 complete protease inhibitor cocktail from Sigma). Supernatant was collected after 12,000 rpm centrifugation for 5 min at 4°C and protein samples with 1 x SDS buffer were loaded on 10% SDS-PAGE gel to detect pMPK3, pMPK4 and pMPK6 by immunoblot with α-pERK1/2 antibody.

BIK1 phosphorylation assay—Protoplasts were isolated from four-week-old WT, *bak1–4*, *cngc20–1* and *bak1–4*/*cngc20–1* plants according to the protocol described previously [51]. 200 μl of protoplasts at the density of 2×10^5/ml for each genotype were transfected with 20 μg of plasmid DNA carrying HA-tagged BIK1 (*pHBT-p35S::BIK1-HA*) at the concentration of 1.8 μg/μl. Protoplasts were incubated at 25°C for 12 hr and treated with or without 100 nM flg22 for 10 min. Samples were subjected for 10% SDS-PAGE and immunoblotting with α-HA-HRP antibody. The flg22-induced BIK1 phosphorylation was evidenced as a mobility shift from immunoblot.

Bacterial infection assay—*Pseudomonas. syringae* pv. *maculicola* ES4326 (*Psm*), *P. syringae* pv. *tomato* (*Pst*) DC3000 (*avrRpt2*), *Pst* DC3000 (*avrRpm1*) and *Pst* DC3000 (*avrRps4*) were cultured for overnight at 28°C in the King's B medium with the appropriate antibiotics (50 μg/ml streptomycin, rifampicin or kanamycin). Bacteria were harvested by centrifugation at 3500 rpm, washed with ddH_2O, and adjusted to the desired density with 10 mM $MgCl_2$. Leaves of four-week-old plants were hand-infiltrated with bacterial suspension using a 1-ml needleless syringe and collected at the indicated time for HR or bacterial growth assays. To measure bacterial growth, two leaf discs were ground in 100 μl H_2O and serial dilutions were plated on TSA medium (1% Bacto tryptone, 1% sucrose, 0.1% glutamic acid, 1.5% agar) with appropriate antibiotics. Bacterial colony forming units (cfu) were counted 2 days and 4 days after inoculation. Each data point is shown as triplicates.

In vivo* co-immunoprecipitation (Co-IP) assay—Arabidopsis* protoplasts were transfected with a pair of constructs tested (the empty vector as the negative control) and incubated for 12 hr. Samples were collected by centrifugation and lysed with Co-IP buffer (20 mM Tris-HCl, pH7.5, 100 mM NaCl, 1 mM EDTA, 10% Glycerol, 0.5% Triton X-100 and protease inhibitor cocktail from Roche) by vertexing. For Co-IP in *Nicotiana benthamiana*, leaves of three-week-old soil-grown plants were hand-infiltrated with different pairs of *Agrobacterium tumefaciens* carrying indicated vectors. Overnight cultured bacteria were harvested by centrifugation and re-suspended in buffer (10 mM MES, pH5.7, 10 mM $MgCl_2$, 200 μM acetosyringone) at OD_{600}=1.5. Leaf samples were harvested two days post-inoculation and subjected to homogenization with Co-IP buffer. Protein extract was pre-incubated with protein-G-agarose beads for 1 hr at 4°C with gentle shaking on a rocker. Immunoprecipitation was carried out with α-FLAG agarose for 3 hr at 4°C. The beads were collected and washed three times with washing buffer (20 mM Tris-HCl, pH7.5, 100 mM NaCl, 1 mM EDTA, 0.1% Triton X-100). The immunoprecipitated proteins and input proteins were analyzed by immunoblotting with indicated antibodies.

***In vitro* pull-down and kinase assays—**Fusion proteins were expressed in *E. coli* BL21 strain using LB medium supplemented with 0.25 mM Isopropyl β-D-1-thiogalactopyranoside (IPTG) [42]. Glutathione-S-transferase (GST), GST-CNGC20N, GST-CNGC20N$^{T145/S146/S183/S184A}$, GST-CNGC20C, GST-CNGC20C^{T560A} and GST-CNGC20C$^{T560/S617/S618/T619A}$ were purified with Pierce glutathione agarose, and maltose binding protein (MBP), MBP-BAK1^{CD} and MBP-BAK1^{CD}KM proteins were purified using amylose resin according to standard protocols. MBP fusion proteins (tagged with HA) were pre-incubated with prewashed glutathione agarose in 300 μL incubation buffer (20 mM Tris-HCl, pH7.5, 100 mM NaCl, 0.1mM EDTA and 0.5% Triton X-100) for 0.5 hr at 4°C. After centrifugation, the supernatant was collected and incubated with prewashed GST, GST-CNGC20N or GST-CNGC20C beads for another 1 hr. The beads were collected and washed three times with washing buffer (20 mM Tris-HCl, pH7.5, 300 mM NaCl, 0.1mM EDTA and 0.1% Triton X-100). Proteins were detected with an α-HA antibody by immunoblotting. For *in vitro* kinase assay, The 1 μg MBP, MBP-BAK1^{CD} or MBP-BAK1^{CD}KM proteins were incubated with 5 μg GST, GST-CNGC20N, GST-CNGC20N$^{T145/S146/S183/S184A}$, GST-CNGC20C, GST-CNGC20C^{T560A} or GST-CNGC20C$^{T560/S617/S618/T619A}$ in the kinase reaction buffer (20 mM Tris-HCl, pH7.5, 20 mM $MgCl_2$, 5 mM EDTA, 1 mM DTT and 100 μM ATP) in the presence of 5 μCi [^{32}P]-γ-ATP for 2 hr at room temperature. The reactions were stopped by adding SDS sample buffer, and protein phosphorylation was visualized by autoradiography in 10% SDS-PAGE.

Mass spectrometry analysis—The *in vitro* phosphorylation for MS analysis was performed in a 20 μl reaction for 2 hr at RT. The reaction buffer contains 20 mM Tris-HCl, pH 7.5, 20 mM $MgCl_2$, 5 mM EDTA, 1 mM DTT, 5 mM ATP, 10 μg GST-CNGC20N or GST-CNGC20C and 1 μg MBP-BAK1^{CD}. The phosphorylated GST-CNGC20N or GST-CNGC20C proteins were resolved by 10% SDS-PAGE gel. The gel was stained with Thermo GelCode Blue Safe Protein Stain and destained with ddH_2O. The corresponding bands were sliced and subjected for in-gel digestion with trypsin. The phosphopeptides were enriched and analyzed using a LTQ Orbitrap XL LC-MS/MS system (Thermo Scientific) as previously described [43]. The MS/MS spectra were analyzed with Mascot (Matrix Science; version 2.2.2), and the identified phosphorylated peptides were manually inspected to ensure confidence in phosphorylation site assignment.

Yeast two-hybrid assay—The plasmids of *pGADT7* (empty vector) or *pGADT7-BAK1^{K}* were introduced into the yeast strain AH109. The plasmids of *pGBKT7* or *pGBKT7-CNGC20N* were introduced into AH109 containing *pGADT7* or *pGADT7-BAK1K*. Polyethylene glycol/LiAc-mediated yeast transformation was performed according to the protocol of Yeastmaker Yeast Transformation System 2 (Clontech). The yeast colonies containing both *pGADT7* and *pGBKT7* were selected on the synthetic defined (SD) medium without leucine and tryptophan (SD-L-T), and the interaction was tested on the SD medium without histidine, leucine and tryptophan (SD-H-L-T), and supplemented with 1 mM 3-amino-1, 2, 4-triazole (3-AT).

Bimolecular fluorescence complementation and subcellular localization assay —Protoplasts from four-week-old WT were transfected with different pairs of BiFC

constructs as shown in the figures. Fluorescence signals in the protoplasts were examined 12 hr after transfection using the Zeiss LSM 780 NLO multiphoton confocal system. YFP and chlorophyll fluorescence signals were excited at 514 and 633 nm respectively. Images were captured in multichannel mode with bright field, and processed with Zeiss ZEN microscope software.

Growth inhibition assay—Four days after germination on 1/2MS plates, *Arabidopsis* seedlings with uniform root lengths were transferred to 24-well culture plates containing 500 μl liquid 1/2MS supplemented without or with 1 μM Pep1. Two seedlings were placed in one well and four repeats were performed. Seedlings were photographed at 7 days after transfer and the root length of individual seedlings were measured.

ROS assay—Around 25 leaves of four-week-old soil-grown *Arabidopsis* plants for each genotype were excised into leaf discs (5-mm diameter) and then cut into leaf strips, followed by an overnight incubation with water in 96-well plates to eliminate the wounding effect. ROS burst was determined by a luminol-based assay. Leaf strips were soaked with solution containing 50 μM luminol and 10 μg/mL horseradish peroxidase supplemented with 100 nM flg22. The measurement was performed immediately after adding the solution with a Multilabel Plate Reader (Perkin-Elmer; Victor X3) for a period of ~35 min. The values for ROS production from each line were indicated as means of relative light units.

Semi-quantification of Ca^{2+} signals—Protoplasts were isolated from four-week-old WT and CRISPR/Cas9 *cngc19*/*cngc20–1* mutants and transfected with *pHBT-p35S::GCaMP3* plasmid DNAs [52, 53]. Protoplasts were incubated at 25°C for 12 hr and transferred to a Greiner 96-well black plate followed by treatment with ddH_2O (Ctrl) or 100 nM flg22. GCaMP3 fluorescence was measured immediately upon treatment using a Perkin Elmer VICTOR X3 Multilabel Plate Reader with an excitation at 485 nm and emission detection at 535 nm. Measurements were recorded for each well at 0.2s intervals, for total duration as indicated in the figures. The difference of the absolute fluorescence value with the control value for each experiment was normalized to the control value as $(F-F_{eq})/F_{eq}$ (where F was the measured fluorescence at a given time point and F_{eq} was the averaged measurement for the samples at the final equilibrated time points measured). Plotted values were averages of five replicate wells, with the SE represented by error bars.

Ca^{2+} yeast mutant complementation—*Saccharomyces cerevisiae* strains W303–1A (WT) and K927 (cch1::TRP1 null mutant) were provided by Dr. H Iida (Tokyo Gakugei University). The Ca^{2+} channel mutant strain K927 was transformed with *pYES2* empty vector, *pYES2-CNGC19*, *pYES2-CNGC20*, or both. To test for complementation of the cch1 mutation, yeast transformants were grown to logarithmic phase in synthetic minimal media and were diluted to 10^6 cells/ml and exposed to 20 μM α-mating factor in modified synthetic minimal media containing 100 μM $CaCl_2$ [34, 54]. 100 μl aliquots of cells were harvested by centrifugation and resuspended in 10 mg/ml Trypan blue solution at various time points. Yeast viability was measured by assessing the ratio of stained to unstained cells under a bright field microscope. A minimum of 200 cells were counted for each transformant.

QUANTIFICATION AND STATISTICAL ANALYSIS

Data for quantification analyses are presented as mean ± standard error (SE) or standard deviation (SD). The statistical analyses were performed by Student's *t*-test or one-way analysis of variance (ANOVA) test (* $P < 0.05$, ** $P < 0.01$, *** $P < 0.001$). Number of replicates is shown in the figure legends.

DATA AND CODE AVAILABILITY

This manuscript did not generate new datasets or code.

Supplementary Material

Refer to Web version on PubMed Central for supplementary material.

ACKNOWLEDGEMENTS

We thank the *Arabidopsis* Biological Resource Center (ABRC) for *Arabidopsis* T-DNA insertion library and various mutant seeds, Dr. Qijun Chen (China Agricultural University, China) for the CRISPR/Cas9 system, Dr. Tim Devarenne for critical reading of the manuscript, and members of the laboratories of L.S. and P.H. for discussions and comments of the experiments. The work was supported by National Institutes of Health (NIH) (R01GM092893) and National Science Foundation (NSF) (IOS-1252539) to P.H, and NIH (R01GM097247) and the Robert A. Welch foundation (A-1795) to L.S. G.X. and W.S. were partially supported by China Scholarship Council (CSC). B.R. was partially supported by Coordenação de Aperfeiçoamento de Pessoal de Nível Superior (CAPS), Brazil.

References:

1. Belkhadir Y, Yang L, Hetzel J, Dangl JL, and Chory J (2014). The growth-defense pivot: crisis management in plants mediated by LRR-RK surface receptors. Trends Biochem Sci 39, 447–456. [PubMed: 25089011]
2. Hohmann U, Lau K, and Hothorn M (2017). The Structural Basis of Ligand Perception and Signal Activation by Receptor Kinases. Annual Review of Plant Biology, Vol 68 68, 109–137.
3. Gomez-Gomez L, and Boller T (2000). FLS2: an LRR receptor-like kinase involved in the perception of the bacterial elicitor flagellin in Arabidopsis. Mol Cell 5, 1003–1011. [PubMed: 10911994]
4. Li J, and Chory J (1997). A putative leucine-rich repeat receptor kinase involved in brassinosteroid signal transduction. Cell 90, 929–938. [PubMed: 9298904]
5. Li J (2010). Multi-tasking of somatic embryogenesis receptor-like protein kinases. Curr Opin Plant Biol 13, 509–514. [PubMed: 20926334]
6. Ma X, Xu G, He P, and Shan L (2016). SERKing Coreceptors for Receptors. Trends Plant Sci 21, 1017–1033. [PubMed: 27660030]
7. Meng X, Chen X, Mang H, Liu C, Yu X, Gao X, Torii KU, He P, and Shan L (2015). Differential Function of Arabidopsis SERK Family Receptor-like Kinases in Stomatal Patterning. Curr Biol 25, 2361–2372. [PubMed: 26320950]
8. Kemmerling B, Schwedt A, Rodriguez P, Mazzotta S, Frank M, Qamar SA, Mengiste T, Betsuyaku S, Parker JE, Mussig C, et al. (2007). The BRI1-associated kinase 1, BAK1, has a brassinolide-independent role in plant cell-death control. Curr Biol 17, 1116–1122. [PubMed: 17583510]
9. He K, Gou X, Yuan T, Lin H, Asami T, Yoshida S, Russell SD, and Li J (2007). BAK1 and BKK1 regulate brassinosteroid-dependent growth and brassinosteroid-independent cell-death pathways. Curr Biol 17, 1109–1115. [PubMed: 17600708]
10. de Oliveira MVV, Xu G, Li B, de Souza Vespoli L, Meng X, Chen X, Yu X, de Souza SA, Intorne AC, de A. Manhães AME, et al. (2016). Specific control of Arabidopsis BAK1/SERK4-regulated cell death by protein glycosylation. Nature Plants 2, 15218. [PubMed: 27250875]

11. Gao M, Liu J, Bi D, Zhang Z, Cheng F, Chen S, and Zhang Y (2008). MEKK1, MKK1/MKK2 and MPK4 function together in a mitogen-activated protein kinase cascade to regulate innate immunity in plants. Cell Res 18, 1190–1198. [PubMed: 18982020]
12. Gao M, Wang X, Wang D, Xu F, Ding X, Zhang Z, Bi D, Cheng YT, Chen S, Li X, et al. (2009). Regulation of cell death and innate immunity by two receptor-like kinases in Arabidopsis. Cell Host Microbe 6, 34–44. [PubMed: 19616764]
13. Talke IN, Blaudez D, Maathuis FJ, and Sanders D (2003). CNGCs: prime targets of plant cyclic nucleotide signalling? Trends Plant Sci 8, 286–293. [PubMed: 12818663]
14. DeFalco TA, Moeder W, and Yoshioka K (2016). Opening the Gates: Insights into Cyclic Nucleotide-Gated Channel-Mediated Signaling. Trends Plant Sci 21, 903–906. [PubMed: 27623305]
15. Pan Y, Chai X, Gao Q, Zhou L, Zhang S, Li L, and Luan S (2019). Dynamic Interactions of Plant CNGC Subunits and Calmodulins Drive Oscillatory Ca(2+) Channel Activities. Dev Cell 48, 710–725 e715. [PubMed: 30713075]
16. Clough SJ, Fengler KA, Yu IC, Lippok B, Smith RK Jr., and Bent AF (2000). The Arabidopsis dnd1 “defense, no death” gene encodes a mutated cyclic nucleotide-gated ion channel. Proc Natl Acad Sci U S A 97, 9323–9328. [PubMed: 10900264]
17. Jurkowski GI, Smith RK Jr., Yu IC, Ham JH, Sharma SB, Klessig DF, Fengler KA, and Bent AF (2004). Arabidopsis DND2, a second cyclic nucleotide-gated ion channel gene for which mutation causes the “defense, no death” phenotype. Mol Plant Microbe Interact 17, 511–520. [PubMed: 15141955]
18. Balague C, Lin B, Alcon C, Flottes G, Malmstrom S, Kohler C, Neuhaus G, Pelletier G, Gaymard F, and Roby D (2003). HLM1, an essential signaling component in the hypersensitive response, is a member of the cyclic nucleotide-gated channel ion channel family. Plant Cell 15, 365–379. [PubMed: 12566578]
19. Ma Y, Walker RK, Zhao YC, and Berkowitz GA (2012). Linking ligand perception by PEPR pattern recognition receptors to cytosolic Ca2+ elevation and downstream immune signaling in plants. Proceedings of the National Academy of Sciences of the United States of America 109, 19852–19857. [PubMed: 23150556]
20. Ali R, Ma W, Lemtiri-Chlieh F, Tsaltas D, Leng Q, von Bodman S, and Berkowitz GA (2007). Death don’t have no mercy and neither does calcium: Arabidopsis CYCLIC NUCLEOTIDE GATED CHANNEL2 and innate immunity. Plant Cell 19, 1081–1095. [PubMed: 17384171]
21. Tian W, Hou C, Ren Z, Wang C, Zhao F, Dahlbeck D, Hu S, Zhang L, Niu Q, Li L, et al. (2019). A calmodulin-gated calcium channel links pathogen patterns to plant immunity. Nature 572, 131–135. [PubMed: 31316205]
22. Meena MK, Prajapati R, Krishna D, Divakaran K, Pandey Y, Reichelt M, Mathew MK, Boland W, Mithofer A, and Vadassery J (2019). The Ca(2+) Channel CNGC19 Regulates Arabidopsis Defense Against Spodoptera Herbivory. Plant Cell 31, 1539–1562. [PubMed: 31076540]
23. Jones JD, and Dangl JL (2006). The plant immune system. Nature 444, 323–329. [PubMed: 17108957]
24. Cui H, Tsuda K, and Parker JE (2015). Effector-triggered immunity: from pathogen perception to robust defense. Annu Rev Plant Biol 66, 487–511. [PubMed: 25494461]
25. Yu X, Feng B, He P, and Shan L (2017). From Chaos to Harmony: Responses and Signaling upon Microbial Pattern Recognition. Annu Rev Phytopathol 55, 109–137. [PubMed: 28525309]
26. Yoshioka K, Moeder W, Kang HG, Kachroo P, Masmoudi K, Berkowitz G, and Klessig DF (2006). The chimeric Arabidopsis CYCLIC NUCLEOTIDE-GATED ION CHANNEL11/12 activates multiple pathogen resistance responses. Plant Cell 18, 747–763. [PubMed: 16461580]
27. Fischer C, Kugler A, Hoth S, and Dietrich P (2013). An IQ domain mediates the interaction with calmodulin in a plant cyclic nucleotide-gated channel. Plant Cell Physiol 54, 573–584. [PubMed: 23385145]
28. Russinova E, Borst JW, Kwaaitaal M, Cano-Delgado A, Yin Y, Chory J, and de Vries SC (2004). Heterodimerization and endocytosis of Arabidopsis brassinosteroid receptors BRI1 and AtSERK3 (BAK1). Plant Cell 16, 3216–3229. [PubMed: 15548744]

29. Lee CH, and MacKinnon R (2017). Structures of the Human HCN1 Hyperpolarization-Activated Channel. Cell 168, 111–120 e111. [PubMed: 28086084]
30. Abdel-Hamid H, Chin K, Moeder W, Shahinas D, Gupta D, and Yoshioka K (2013). A suppressor screen of the chimeric AtCNGC11/12 reveals residues important for intersubunit interactions of cyclic nucleotide-gated ion channels. Plant Physiol 162, 1681–1693. [PubMed: 23735507]
31. Chiasson DM, Haage K, Sollweck K, Brachmann A, Dietrich P, and Parniske M (2017). A quantitative hypermorphic CNGC allele confers ectopic calcium flux and impairs cellular development. eLife 6.
32. Moeder W, Urquhart W, Ung H, and Yoshioka K (2011). The role of cyclic nucleotide-gated ion channels in plant immunity. Mol Plant 4, 442–452. [PubMed: 21459831]
33. Wang J, Liu X, Zhang A, Ren Y, Wu F, Wang G, Xu Y, Lei C, Zhu S, Pan T, et al. (2019). A cyclic nucleotide-gated channel mediates cytoplasmic calcium elevation and disease resistance in rice. Cell Res.
34. Chin K, Moeder W, Abdel-Hamid H, Shahinas D, Gupta D, and Yoshioka K (2010). Importance of the alphaC-helix in the cyclic nucleotide binding domain for the stable channel regulation and function of cyclic nucleotide gated ion channels in Arabidopsis. J Exp Bot 61, 2383–2393. [PubMed: 20378667]
35. Boudsocq M, and Sheen J (2010). Stress Signaling II: Calcium Sensing and Signaling. Abiotic Stress Adaptation in Plants: Physiological, Molecular and Genomic Foundation, 75–90.
36. Chin K, DeFalco TA, Moeder W, and Yoshioka K (2013). The Arabidopsis cyclic nucleotide-gated ion channels AtCNGC2 and AtCNGC4 work in the same signaling pathway to regulate pathogen defense and floral transition. Plant Physiol 163, 611–624. [PubMed: 24027242]
37. Ladwig F, Dahlke RI, Stuhrwohldt N, Hartmann J, Harter K, and Sauter M (2015). Phytosulfokine Regulates Growth in Arabidopsis through a Response Module at the Plasma Membrane That Includes CYCLIC NUCLEOTIDE-GATED CHANNEL17, H+-ATPase, and BAK1. Plant Cell 27, 1718–1729. [PubMed: 26071421]
38. Yamada K, Saijo Y, Nakagami H, and Takano Y (2016). Regulation of sugar transporter activity for antibacterial defense in Arabidopsis. Science 354, 1427–1430. [PubMed: 27884939]
39. Lin W, Li B, Lu D, Chen S, Zhu N, He P, and Shan L (2014). Tyrosine phosphorylation of protein kinase complex BAK1/BIK1 mediates Arabidopsis innate immunity. Proc Natl Acad Sci U S A 111, 3632–3637. [PubMed: 24532660]
40. Du JB, Gao Y, Zhan YY, Zhang SS, Wu YJ, Xiao Y, Zou B, He K, Gou XP, Li GJ, et al. (2016). Nucleocytoplasmic trafficking is essential for BAK1-and BKK1-mediated cell-death control. Plant Journal 85, 520–531. [PubMed: 26775605]
41. Shan LB, He P, Li JM, Heese A, Peck SC, Nurnberger T, Martin GB, and Sheen J (2008). Bacterial effectors target the common signaling partner BAK1 to disrupt multiple MAMP receptor-signaling complexes and impede plant immunity. Cell Host & Microbe 4, 17–27. [PubMed: 18621007]
42. Li B, Jiang S, Yu X, Cheng C, Chen S, Cheng Y, Yuan JS, Jiang D, He P, and Shan L (2015). Phosphorylation of Trihelix Transcriptional Repressor ASR3 by MAP KINASE4 Negatively Regulates Arabidopsis Immunity. The Plant cell 27, 839–856. [PubMed: 25770109]
43. Gao X, Chen X, Lin W, Chen S, Lu D, Niu Y, Li L, Cheng C, McCormack M, Sheen J, et al. (2013). Bifurcation of Arabidopsis NLR immune signaling via Ca(2)(+)-dependent protein kinases. PLoS Pathog 9, e1003127. [PubMed: 23382673]
44. Li F, Cheng C, Cui F, de Oliveira MV, Yu X, Meng X, Intorne AC, Babilonia K, Li M, Li B, et al. (2014). Modulation of RNA Polymerase II Phosphorylation Downstream of Pathogen Perception Orchestrates Plant Immunity. Cell Host Microbe.
45. Lu D, Wu S, Gao X, Zhang Y, Shan L, and He P (2010). A receptor-like cytoplasmic kinase, BIK1, associates with a flagellin receptor complex to initiate plant innate immunity. Proceedings of the National Academy of Sciences of the United States of America 107, 496–501. [PubMed: 20018686]
46. Nour-Eldin HH, Hansen BG, Nørholm MHH, Jensen JK, and Halkier BA (2006). Advancing uracil-excision based cloning towards an ideal technique for cloning PCR fragments. Nucleic acids research 34, e122–e122. [PubMed: 17000637]

47. Xing HL, Dong L, Wang ZP, Zhang HY, Han CY, Liu B, Wang XC, and Chen QJ (2014). A CRISPR/Cas9 toolkit for multiplex genome editing in plants. BMC Plant Biol 14, 327. [PubMed: 25432517]

48. Mang H, Feng B, Hu Z, Boisson-Dernier A, Franck CM, Meng X, Huang Y, Zhou J, Xu G, Wang T, et al. (2017). Differential Regulation of Two-Tiered Plant Immunity and Sexual Reproduction by ANXUR Receptor-Like Kinases. The Plant cell 29, 3140–3156. [PubMed: 29150546]

49. Yao X, Horie T, Xue S, Leung HY, Katsuhara M, Brodsky DE, Wu Y, and Schroeder JI (2009). Differential Sodium and Potassium Transport Selectivities of the Rice OsHKT2;1 and OsHKT2;2 Transporters in Plant Cells. Plant physiology 152, 341–355. [PubMed: 19889878]

50. Langmead B, and Salzberg SL (2012). Fast gapped-read alignment with Bowtie 2. Nat Methods 9, 357–U354. [PubMed: 22388286]

51. He P, Shan L, and Sheen J (2007). The use of protoplasts to study innate immune responses. Methods Mol Biol 354, 1–9. [PubMed: 17172739]

52. DeFalco TA, Toyota M, Phan V, Karia P, Moeder W, Gilroy S, and Yoshioka K (2017). Using GCaMP3 to Study Ca2+ Signaling in Nicotiana Species. Plant Cell Physiol 58, 1173–1184. [PubMed: 28482045]

53. Toyota M, Spencer D, Sawai-Toyota S, Jiaqi W, Zhang T, Koo AJ, Howe GA, and Gilroy S (2018). Glutamate triggers long-distance, calcium-based plant defense signaling. Science 361, 1112–1115. [PubMed: 30213912]

54. Muller EM, Locke EG, and Cunningham KW (2001). Differential regulation of two Ca(2+) influx systems by pheromone signaling in Saccharomyces cerevisiae. Genetics 159, 1527–1538. [PubMed: 11779794]

Highlights:

1. CNGC20 specifically regulates *bak1/serk4* cell death.
2. BAK1 phosphorylates CNGC20 and regulates CNGC20 stability.
3. CNGC19 contributes to *bak1/serk4* cell death in the absence of CNGC20.
4. CNGC20 and CNGC19 form complexes and are Ca^{2+} permeable channels.

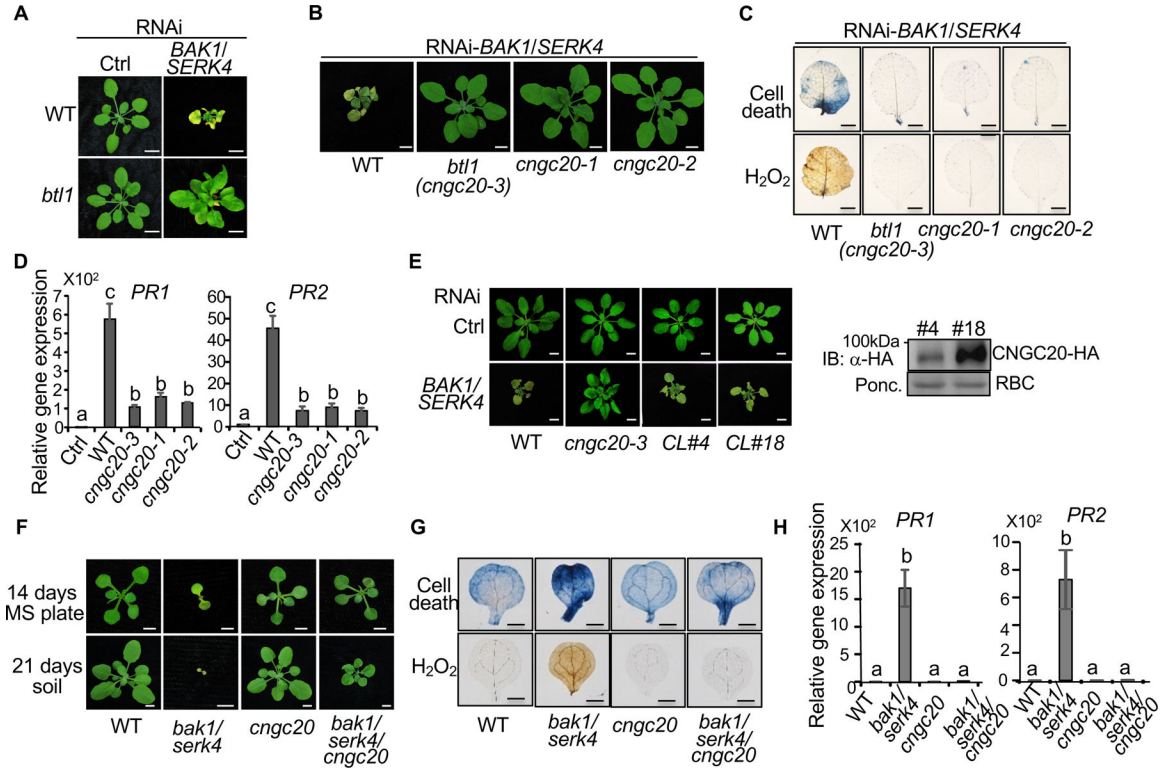

Figure 1. The *cngc20* mutants suppress *bak1/serk4* cell death.

(A) The *btl1* mutant suppresses growth defects triggered by RNAi-*BAK1/SERK4*. Plant phenotypes are shown two weeks after VIGS of *BAK1/SERK4* or a vector control (Ctrl). Bar=5 mm.

(B) The *cngc20* mutants suppress growth defects triggered by RNAi-*BAK1/SERK4*. Plant phenotypes are shown for WT, *btl1* (*cngc20–3*), *cngc20–1*, and *cngc20–2* two weeks after VIGS of *BAK1/SERK4*. Bar=5 mm.

(C) The *cngc20* mutants suppress cell death and H_2O_2 production triggered by RNAi-*BAK1/SERK4*. Plant true leaves after VIGS of *BAK1/SERK4* were stained with trypan blue for cell death (top panel) and DAB for H_2O_2 accumulation (bottom panel). Bar=2 mm.

(D) The *cngc20* mutants suppress *PR1* and *PR2* expression triggered by RNAi-*BAK1/SERK4*. The expression of *PR1* and *PR2* was normalized to the expression of *UBQ10*. The data are shown as mean ± SE from three independent repeats. The different letters denote statistically significant difference according to one-way ANOVA followed by Tukey test ($p<0.05$).

(E) Complementation of *cngc20–3* with the *CNGC20* genomic fragment (*gCNGC20*) under its native promoter restores growth defects by RNAi-*BAK1/SERK4*. CL#4 and CL#18 are two representative lines. Bar=5 mm. The HA epitope tagged CNGC20 proteins in transgenic plants were detected with an α-HA immunoblot (IB). Protein loading is shown by Ponceau S staining (Ponc.) for RuBisCo (RBC).

(F) The *cngc20–3* mutant partially rescues the seedling lethality of *bak1–4/serk4–1*. Seedlings were grown on 1/2MS plate and photographed at 14 days post-germination (dpg) (top panel, Bar=2 mm.) or in soil and photographed at 21 dpg (bottom panel, Bar=5 mm). The *bak1–4/serk4–1* mutant was photographed at 14 dpg and dead at 21 dpg.

(G) Alleviation of cell death and H_2O_2 accumulation in *bak1–4/serk4–1/cngc20–3* compared to *bak1–4/serk4–1*. Bar=1 mm.

(H) Reduced *PR1* and *PR2* expression in *bak1–4/serk4–1/cngc20–3* compared to *bak1–4/serk4–1*. The different letters denote statistically significant difference according to one-way ANOVA followed by Tukey test ($p<0.05$). The above experiments were repeated at least three times with similar results.

See also Figure S1, S2, Table S1 and S2.

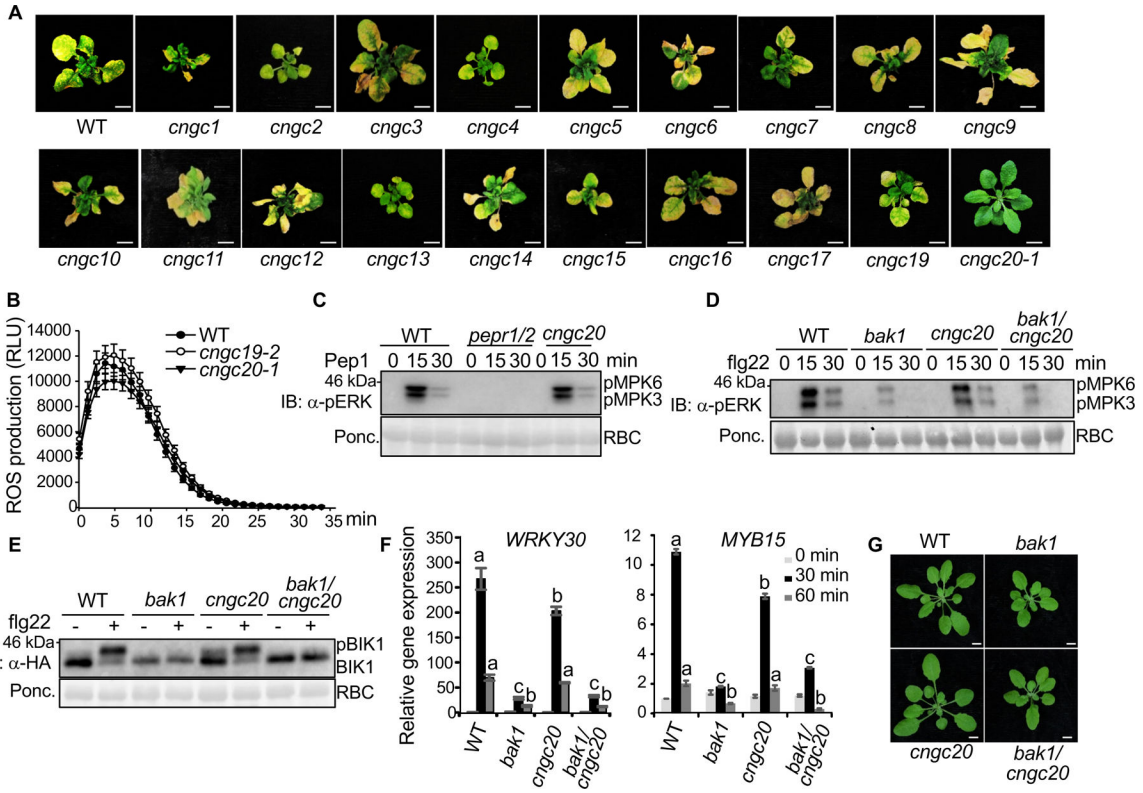

Figure 2. Specific function of CNGC20 in *bak1/serk4* cell death.

(A) Unlike *cngc20–1*, other *cngc* mutants do not suppress growth defects by RNAi-*BAK1/SERK4*. Plant phenotypes are shown two weeks after VIGS of *BAK1/SERK4*. Bar=1 cm.

(B) The *cngc19* and *cngc20* mutants exhibit similar flg22-induced ROS production as WT plants. Leave discs from four-week-old WT, *cngc19–2* and *cngc20–1* plants were treated with 100 nM flg22 for 35 min. The data are shown as means ± SE from 24 leaf discs.

(C) The *cngc20–3* mutant exhibits similar Pep1-induced MAPK activation as WT. Ten-day-old seedlings were treated without or with 100 nM Pep1 for 15 and 30 min. The MAPK activation was analyzed by immunoblot with α-pERK antibody (top panel), and the protein loading is shown by Ponceau S staining for RBC (bottom panel). The *pepr1/2* is the Pep1 receptor PEPR1 and PEPR2 double mutant.

(D) The *cngc20–1* mutant does not interfere with the compromised flg22-induced MAPK activation in *bak1–4*. Ten-day-old seedlings were treated without or with 100 nM flg22 for 15 and 30 min. MAPK activation was analyzed by immunoblotting with α-pERK antibody (top panel), and protein loading is shown by Ponceau S staining for RBC (bottom panel).

(E) The *cngc20–1* mutant does not affect the compromised flg22-induced BIK1 phosphorylation in *bak1–4*. Protoplasts from different plants were transfected with HA-tagged BIK1 and treated with 100 nM flg22 for 10 min. BIK1-HA proteins were detected by immunoblotting using α-HA antibody (top panel), and protein loading is shown by Ponceau S staining for RBC (bottom panel).

(F) The *cngc20–1* mutant did not affect the compromised flg22-induced gene expression in *bak1–4*. Ten-day-old seedlings were treated without or with 100 nM flg22 for 30 or 60 min for qRT-PCR analysis. The data are shown as mean ± SE from three independent repeats.

The different letters indicate statistically significant differences from WT within the same time point according to two-way ANOVA followed by Tukey test ($p<0.05$).

(G) The *cngc20–1* mutant does not affect the growth phenotype of *bak1–4*. Four-week-old soil-grown plants are shown. The *cngc20–1/bak1–4* mutant exhibited similar growth phenotypes, including rounder leaves and shorter petioles, as *bak1–4* compared to WT plants. Bar=5 mm.

The above experiments were repeated at least three times with similar results.

See also Figure S3, S4 and Table S3.

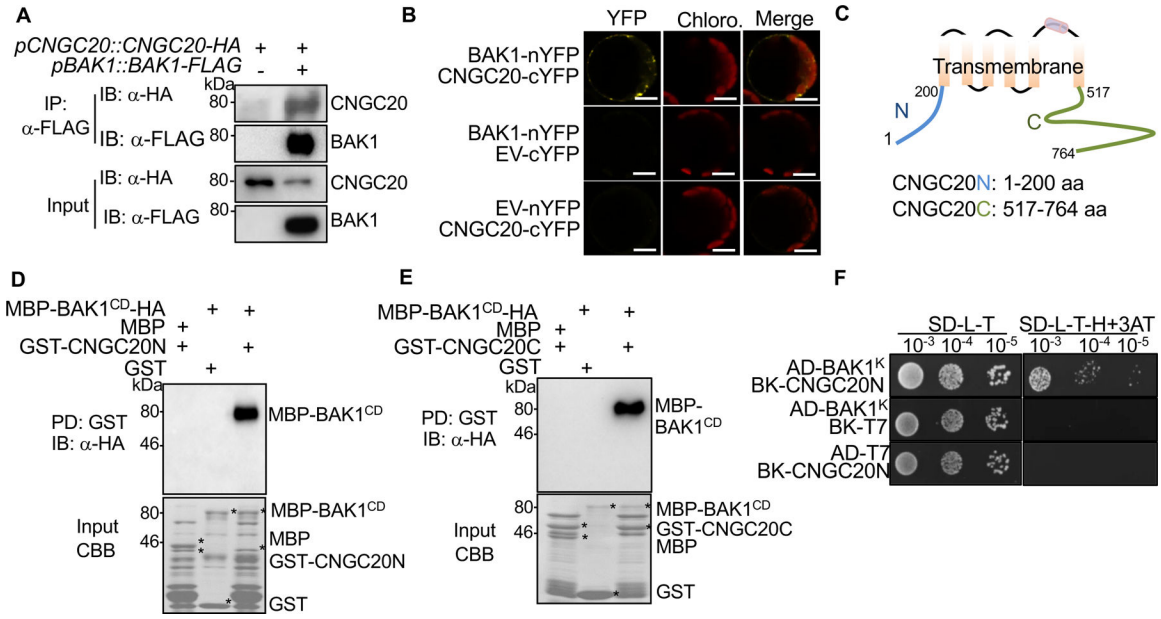

Figure 3. BAK1 interacts with CNGC20.

(A) CNGC20 associates with BAK1 in transgenic plants. Protein extracts from transgenic plants carrying *pBAK1::BAK1-FLAG* and *pCNGC20::CNGC20-HA* were immunoprecipitated with α-FLAG agarose beads (IP: α-FLAG) and immunoblotted with α-HA (IB: α-HA) or α-FLAG (IB: α-FLAG) (top two panels). Protein inputs are shown with immunoblotting before immunoprecipitation (bottom two panels).

(B) Interaction between CNGC20 and BAK1 by BiFC assay in *Arabidopsis* protoplasts. BAK1-nYFP (BAK1 fused with N-terminal YFP) and CNGC20-cYFP (CNGC20 fused with C-terminal YFP) proteins were transiently co-expressed in protoplasts. YFP signals were observed using a confocal microscopy. EV indicates the empty vector control. Bar=10 μm.

(C) Schematic diagram of CNGC20 protein structure indicating the transmembrane and cytosolic N-terminal and C-terminal domains (hereafter, CNGC20N and CNGC20C).

(D) CNGC20N interacts with the BAK1 cytosolic domain ($BAK1^{CD}$) in an *in vitro* pull-down (PD) assay. GST or GST-CNGC20N immobilized on glutathione sepharose beads was incubated with MBP or MBP-$BAK1^{CD}$-HA proteins. The beads were washed and pelleted for immunoblotting with α-HA antibody (PD: GST; IB: α-HA) (top panel). Coomassie blue staining (CBB) of input proteins is shown on the bottom.

(E) CNGC20C interacts with $BAK1^{CD}$ *in vitro*. A similar assay using CNGC20C was performed as in (D).

(F) The BAK1 kinase domain ($BAK1^{K}$) interacts with CNGC20N in a yeast two-hybrid assay. The interaction between $BAK1^{K}$ and CNGC20N was tested on synthetic defined (SD) medium without leucine, tryptophan and histidine (SD-L-T-H) supplemented with 1 mM 3-amino-1, 2, 4-triazole (3AT). *pGADT7* and *pGBKT7* are empty vectors. Serial dilutions of the yeast colonies were plated.

The above experiments were repeated three times with similar results.

See also Figure S5.

A

Phosphopeptides from CNGC20C

Peptide	Cover region	Identified Site	Expect	Score	Dupes
NLEMTLR	521-528	Thr^{526}	0.06	26	2
DVEQWMSHR	530-539	Ser^{537}	1.3	13	1
FNWAATR	554-561	Thr^{560}	0.04	36	1
TYIGSSTVLHR	612-623	Ser^{617}	0.06	36	0
TYIGSSTVLHR	612-623	Ser^{618}	e-5	56	0
TYIGSSTVLHR	612-623	Thr^{619}	0.1	26	1
SSVNPDGTRIR	667-678	Thr^{675}	0.1	32	2

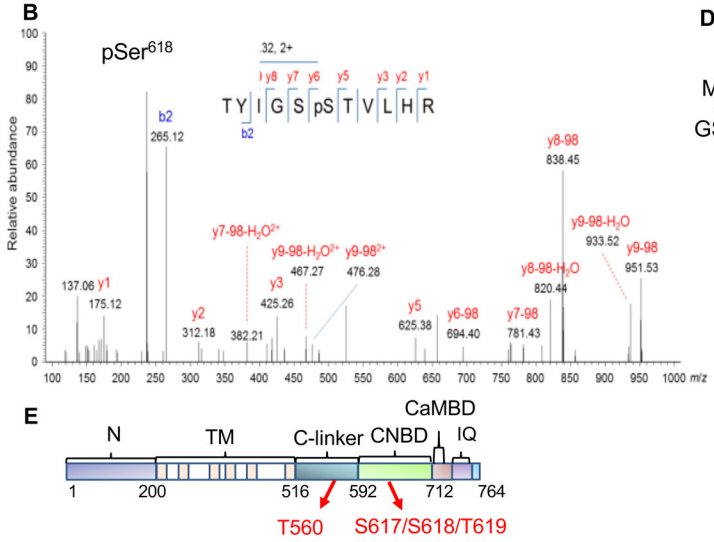

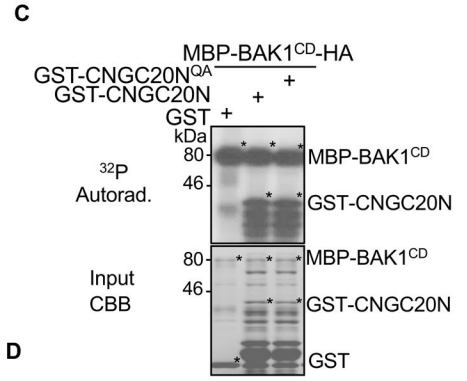

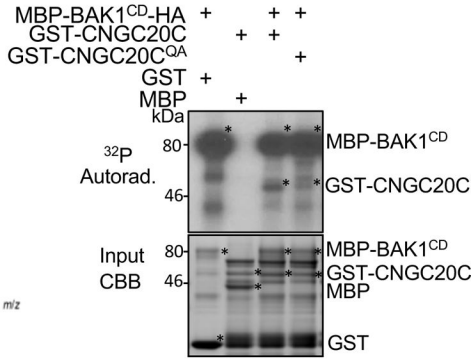

Figure 4. BAK1 phosphorylates CNGC20.

(A) Phosphorylation sites and the corresponding phosphopeptides from CNGC20C region identified from LC-MS/MS analysis. Expect indicates the number of times the peptide is matched by chance (the smaller this value is, the more significant the peptide identification is). Score is a measure of how well the experimental MS/MS spectrum matches to the stated peptide based on calculated probability (P) that the observed match is random. The reported score is: −10Log(P) (the higher the value is, the more confident the peptide identification is). Dupes is the number of additional matches to the same peptide with the same modifications and charge.

(B) LC-MS/MS analysis reveals that Ser^{618} of CNGC20C is phosphorylated by BAK1^{CD}.

(C) The Thr^{155A}/Ser^{156A}/Ser^{183A}/Ser^{184A} quadruple mutant of CNGC20N (CNGC20N^{QA}) does not affect its phosphorylation by BAK1 (top panel). The kinase assay was performed by incubating MBP-BAK1^{CD} with GST, GST-CNGC20N or GST-CNGC20N^{QA} as a substrate. Phosphorylation of CNGC20N by BAK1^{CD} is shown with autoradiography (top panel). Protein loading control is shown by CBB (bottom panel).

(D) The Thr^{560A}/Ser^{617A}/Ser^{618A}/Thr^{619A} quadruple mutant of CNGC20C (CNGC20C^{QA}) compromises its phosphorylation by BAK1^{CD} (top panel). A similar assay using GST-CNGC20C or GST-CNGC20C^{QA} was performed as in (C).

(E) Schematic diagram of the CNGC20 protein motifs with identified phosphorylation sites. Cytoplasmic N-terminus (N, 1–200); transmembrane region (TM, 201–516); C-linker (517–592); cyclic nucleotide binding domain (CNBD, 593–712); calmodulin binding domain

(CaMBD, 713–732); IQ domain (737–752). Numbers indicate amino acid positions. The two red arrows indicate locations of phosphorylation residues.

The above experiments, except LC-MS/MS, were repeated three times with similar results. See also Figure S5 and S6.

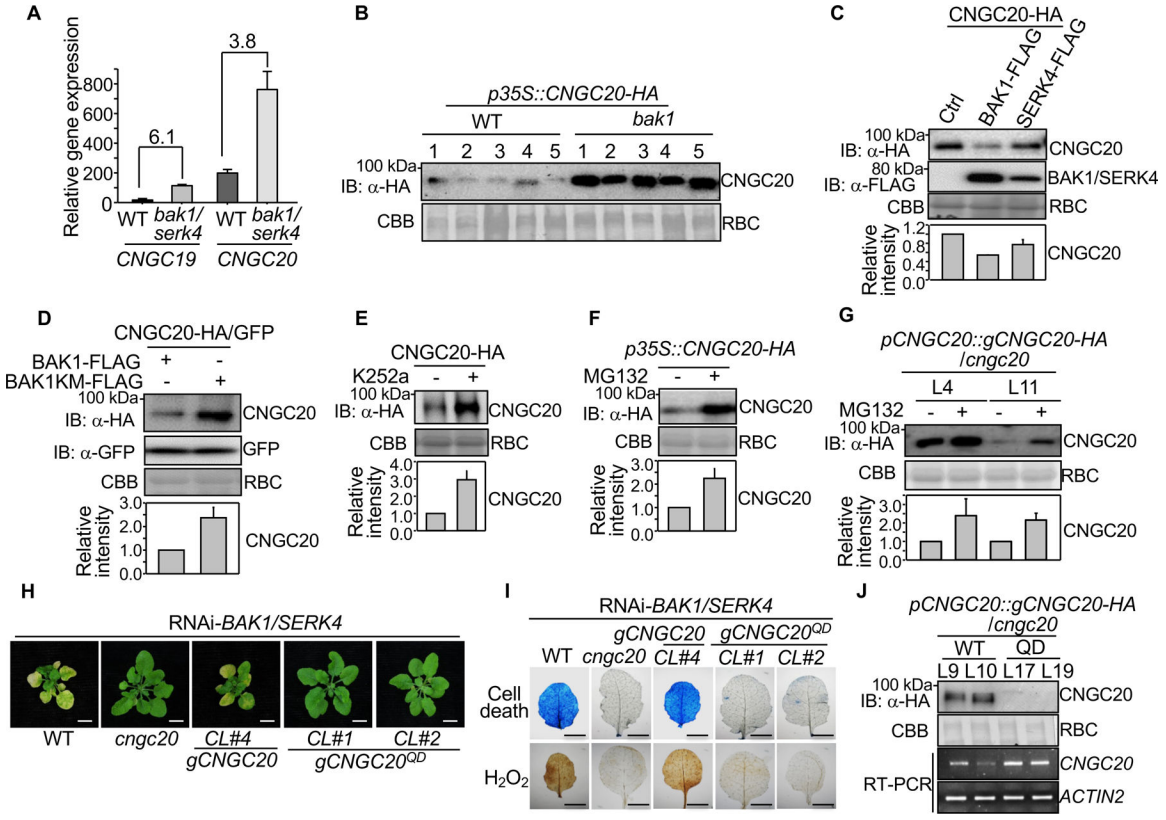

Figure 5. BAK1 destabilizes CNGC20 through phosphorylation.

(A) Transcripts of *CNGC19* and *CNGC20* are upregulated in *bak1–4/serk4–1*. Mean gene expression levels of *CNGC19* and *CNGC20* in *bak1–4/serk4–1* and WT were obtained from RNA-Seq data [10]. The data are shown as mean ± SD from two independent repeats. The numbers indicate fold changes of gene expression (*bak1–4/serk4–1* vs. WT).

(B) BAK1 is required for CNGC20 destabilization. The *CNGC20* cDNA fragment with a C-terminal HA tag under the *35S* promoter was introduced into WT or *bak1–4*. About 20 independent T_1 transgenic lines were obtained and five representative lines from each background are shown for immunoblot analysis with α-HA.

(C) CNGC20 proteins are destabilized by co-expression with BAK1 or SERK4. CNGC20-HA was co-expressed with empty vector (Ctrl), BAK1-FLAG or SERK4-FLAG in *Arabidopsis* protoplasts for 12 hr. Protein expression was analyzed with α-HA or α-FLAG immunoblot.

(D) BAK1, not the BAK1 kinase mutant (BAK1KM), destabilizes CNGC20 proteins. CNGC20-HA or GFP proteins were co-expressed with BAK1-FLAG or BAK1KM-FLAG in *Arabidopsis* protoplasts for 12 hr. Protein expression was analyzed with α-HA or α-GFP immunoblot.

(E) Pretreatment of kinase inhibitor K252a stabilizes CNGC20-HA in *Arabidopsis* protoplasts. Protoplasts expressing CNGC20-HA were treated with 0.05% DMSO (−) or 1 μM K252a for 12 hr. Protein expression was analyzed with α-HA immunoblot.

(F) The protein degradation inhibitor MG132 stabilizes CNGC20-HA proteins in *N. benthamiana*. CNGC20-HA was expressed in *N. benthamiana* by *Agrobacterium*-mediated transient assay. 0.1% DMSO (−) or 2 μM MG132 was infiltrated 3 hr before the samples

were collected at two days post-inoculation (dpi). Total proteins were analyzed by immunoblot with α-HA.

(G) Stabilization of CNGC20-HA proteins by MG132 in transgenic plants. Ten-day-old *pCNGC20::gCNGC20-HA/cngc20–1* seedlings were pretreated with 0.1% DMSO (−) or 2 μM MG132 for 3 hr before total proteins were isolated for immunoblot analysis with α-HA. Quantifications of CNGC20-HA relative intensity from the immunoblots (IB) are shown on the bottom in (C), (D), (E), (F) and (G) as mean ± SE from three independent repeats. The intensity of CNGC20-HA band normalized to RBC by CBB staining in the first lane in (C) and (D), and the non-treatment in (E), (F) and (G) was set as 1.0.

(H) Complementation of *cngc20–1* with the $Thr^{560D}/Ser^{617D}/Ser^{618D}/Thr^{619D}$ quadruple mutant of *CNGC20* genomic fragment (*gCNGC20*^{QD}) under its native promoter does not restore growth defects by RNAi-*BAK1/SERK4*. CL#1 and CL#2 are two representative lines. Bar=5 mm. CL#4 is the complementation line with WT CNGC20.

(I) The $CNGC20^{QD}$ mutant does not restore cell death and H_2O_2 production triggered by RNAi-*BAK1/SERK4*. True leaves of WT, *cngc20–1*, *CNGC20* (*CL#4*) and *CNGC20*^{QD} (CL#1 and CL#2) after RNAi-*BAK1/SERK4* were stained with trypan blue for cell death (top panel) and DAB for H_2O_2 accumulation (bottom panel). Bar=2 mm.

(J) CNGC20-HA proteins accumulate more than $CNGC20^{QD}$-HA proteins in transgenic plants. Plants from two independent homozygous T_3 lines of *pCNGC20::gCNGC20-HA/cngc20–1* and *pCNGC20::gCNGC20*^{QD}*-HA/cngc20–1* were subjected to immunoblot with α-HA antibody. RT-PCR was performed with *CNGC20* specific primers to detect the transcript level of *CNGC20* and *CNGC20*^{QD}. *ACTIN2* was used as an internal control. The above experiments, except A, were repeated three times with similar results.

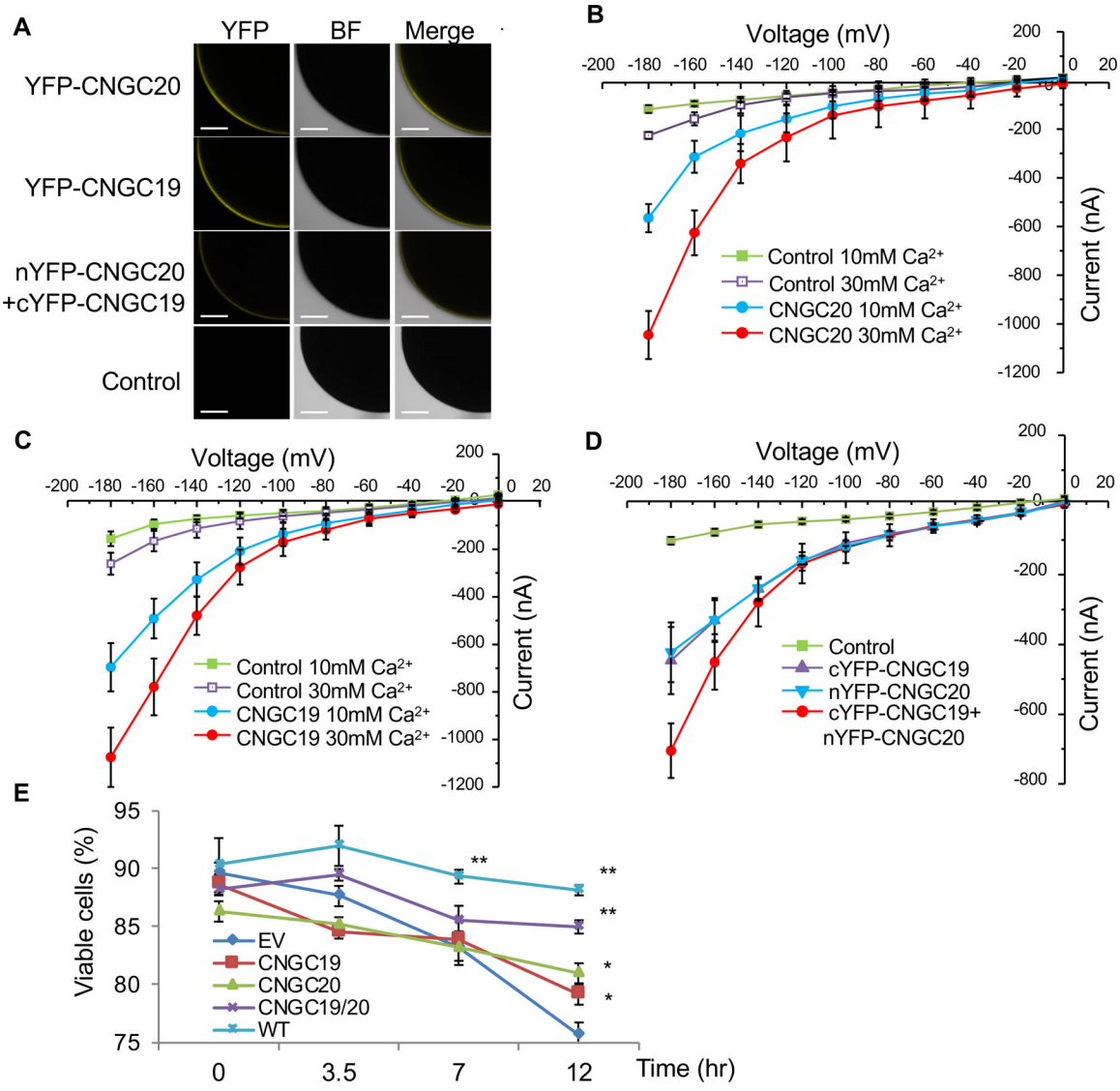

Figure 6. CNGC20 and CNGC19 are Ca^{2+}-permeable channels.

(A) Confocal fluorescence images of oocytes expressing YFP-CNGC20, YFP-CNGC19 or co-expressing nYFP-CNGC20 (N-terminal YFP fused with CNGC20) and cYFP-CNGC19 (C-terminal YFP fused with CNGC19). Water-injected control is showed on the bottom. YFP signals were observed using a confocal microscopy. BF indicates bright field. Bar=200 μm.

(B) CNGC20 exhibits Ca^{2+}-permeable channel activity in *Xenopus* oocyte. Current-voltage relationship was recorded in oocytes expressing YFP-CNGC20 in the presence of $CaCl_2$. Voltage steps of 0 to −180 mV in 20 mV decrements. Data shown are means ± SE, Control in 10 mM $CaCl_2$ (n = 8) or 30 mM $CaCl_2$ (n=5), CNGC20 in 10 mM $CaCl_2$ (n = 8) or 30 mM $CaCl_2$ (n = 8).

(C) CNGC19 exhibits Ca^{2+}-permeable channel activity when expressed in *Xenopus* oocytes. Current-voltage relationship was recorded in oocytes expressing YFP-CNGC19 in the presence of $CaCl_2$. Voltage steps of 0 to −180 mV in 20 mV decrements. Data shown are

means ± SE, Control in 10 mM $CaCl_2$ (n = 10) or 30 mM $CaCl_2$ (n=8), CNGC19 in 10 mM $CaCl_2$ (n=15) or 30 mM $CaCl_2$ (n = 9).

(D) CNGC19 and CNGC20 additively enhance channel activity in *Xenopus* oocyte. Current-voltage relationship was recorded in oocytes injected with water control (n=6), cYFP-CNGC19 (n=7), nYFP-CNGC20 (n=7), or cYFP-CNGC19+nYFP-CNGC20 (n=12) in the presence of 10 mM $CaCl_2$.

(E) Enhanced Ca^{2+}-permeable channel activity of CNGC19/CNGC20 in yeast complementation analysis. CNGC19/CNGC20 complemented the Ca^{2+}-uptake deficient mutant K927 (cchl::TRP1). Time course after addition of 20 μM α-mating factor is shown. Each data point is average of three independent samples (=independent yeast transformation colony). 200 cells were scored and the percentage of viable cells was calculated.

The above experiments were repeated three times with similar results.

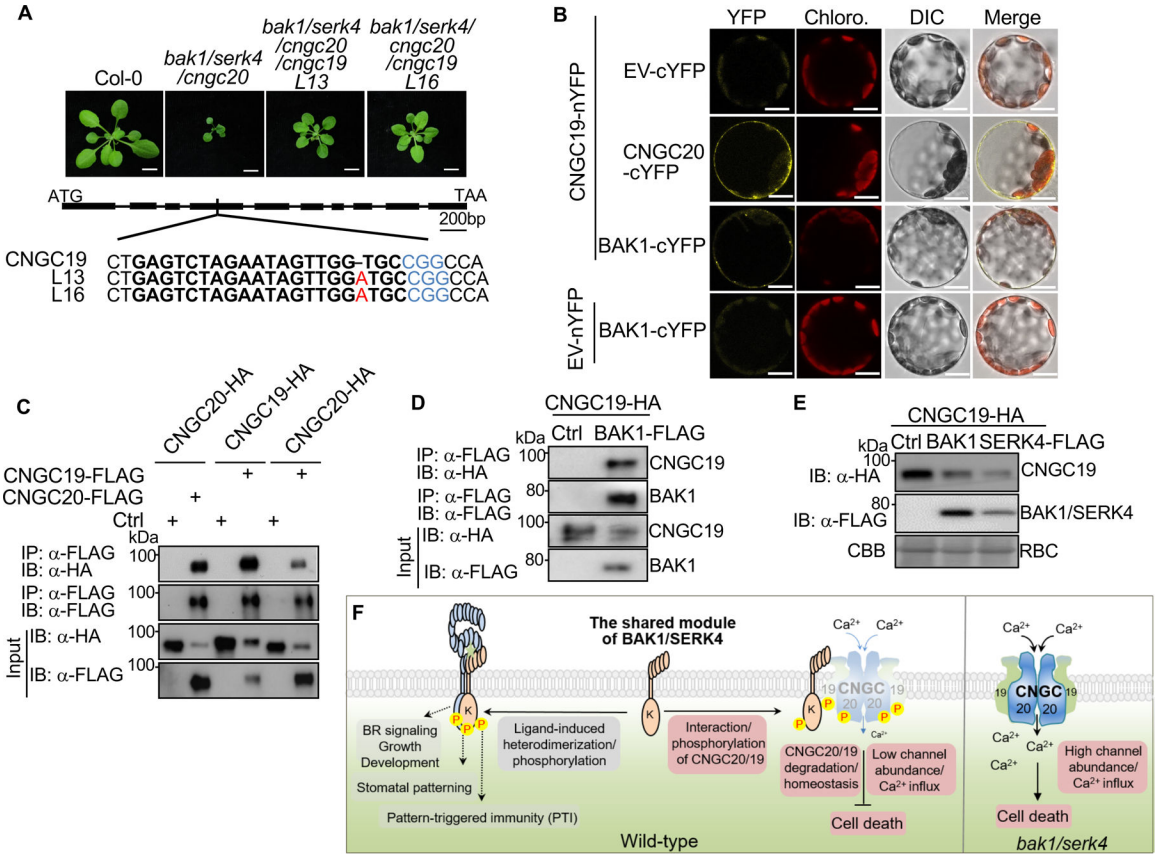

Figure 7.

CNGC20 and CNGC19 heteromerize and contribute additively to *bak1/serk4* cell death

(A) The CRISPR/Cas9 *cngc19* mutants further rescue the growth defect of *bak1–4/serk4–1/cngc20–1*. Plants grown in soil were photographed at 21 dpg. Bar=1 cm. Scheme of *CNGC19* with the gene editing site is shown below. Solid bars indicate exons and lines indicate introns. Both line13 and line16 of the quadruple mutants carry an adenine insertion (red) in the fourth exon of *CNGC19*. Selected target sequences (20 base pairs) are shown in bold and protospacer adjacent motif (PAM) sequences are shown in blue.

(B) CNGC19 associates with CNGC20 and BAK1 in a BiFC assay. CNGC19-nYFP was co-expressed with EV-cYFP, CNGC20-cYFP, or BAK1-cYFP in *Arabidopsis* protoplasts. Reconstructed YFP signals were observed using a confocal microscopy 12 hr after transfection. EV indicates the empty vector. Bar=10 μm.

(C) Homo- and heteromerization of CNGC19 and CNGC20 in *Arabidopsis* protoplasts. Proteins were transiently co-expressed in *Arabidopsis* protoplasts and subjected for immunoprecipitation assays with α-FLAG agarose beads for IP and with α-HA or α-FLAG for IB (top two panels). The input control is shown on the bottom two panels.

(D) CNGC19 associates with BAK1 in *Arabidopsis* protoplasts. BAK1-FLAG and CNGC19-HA proteins were transiently co-expressed in *Arabidopsis* protoplasts. Co-IP was performed as in (C).

(E) CNGC19 proteins are destabilized by co-expression with BAK1 or SERK4. CNGC19-HA was co-expressed with Ctrl, BAK1-FLAG or SERK4-FLAG in *Arabidopsis* protoplasts for 12 hr. Protein expression was analyzed with α-HA or α-FLAG immunoblot.
(F) A model for cell death regulation by BAK1/SERK4-mediated phosphorylation of CNGC20/CNGC19. As a shared module, BAK1/SERK4 regulate plant growth, development, and immunity via ligand-induced heterodimerization and transphosphorylation with their cognate receptor kinases. Unique to cell death regulation, BAK1/SERK4 associate with and phosphorylate the plasma membrane-localized Ca^{2+} permeable channels CNGC20/CNGC19. Specific phosphorylation at the C-terminal cytosolic domain modulates the degradation of the CNGC20/CNGC19 complex and cellular homeostasis. In the *bak1/serk4* mutant, without BAK1/SERK4 phosphorylation, CNGC20/CNGC19 are overproduced, leading to mis-regulation of Ca^{2+} influx and downstream signaling, eventually causing cell death. The abundance of CNGC20 is likely more than CNGC19.
The above experiments were repeated three times with similar results.
See also Figure S7.

KEY RESOURCES TABLE

REAGENT or RESOURCE	SOURCE	IDENTIFIER
Antibodies		
Anti-HA-Peroxidase	Roche	Cat # 12013819001; RRID:AB_439705
Anti-FLAG-Peroxidase	Sigma-Aldrich	Cat # A8592; RRID:AB_259529
Anti-GFP	Roche	Cat # 11814460001; RRID:AB_390913
Anti-Mouse IgG HRP-linked antibody	Cell Signaling	Cat # 7076; RRID:AB_330924
Phospho-p44/42 MAPK (Erk1/2) Antibody	Cell Signaling	Cat #9101; RRID:AB_331646
Anti-rabbit IgG HRP-linked antibody	Cell Signaling	Cat #7074; RRID:AB_2099233
Anti-FLAG M2 Affinity gel	Sigma-Aldrich	Cat # 2220; RRID:AB_10063035
Protein G Agarose	Roche	Cat # 05015952001
Bacterial and Virus Strains		
Agrobacterium tumefaciens GV3101	[10]	N/A
E. coli BL21	[42]	N/A
Pseudomonas syringae pv. *tomato* DC3000 (*Pst*)	[41]	N/A
P. syringae pv. *maculicola* ES4326 (*Psm*)	[44]	N/A
Pst avrRpt2	[42]	N/A
Pst avrRpm1	[43]	N/A
Pst avrRps4	[43]	N/A
Chemicals, Peptides, and Recombinant Proteins		
flg22	[48]	N/A
Pep1	[48]	N/A
MG132	AG Scientific	Cat #99533-80-9
K252a	AG Scientific	Cat #133407-82-6
RiboZol™ RNA Extraction Reagent	AMRESCO	Cat # N580
IPTG	Sigma-Aldrich	Cat# I6758
Pierce glutathione agarose	Thermo Scientific	Cat# 16101
amylose resin	New England BioLabs	Cat# E8021L
Luminol	Sigma-Aldrich	Cat#A8511
Peroxidase from horseradish	Sigma-Aldrich	Cat#P6782
RNase-free DNase I	New England BioLabs	Cat # M0303L
Critical Commercial Assays		
M-MuLV Reverse Transcriptase	New England BioLabs	Cat # M0253L
iTaq SYBR green Supermix	Bio-Rad	Cat # 1725124
mMESSAGE mMACHINE T7 high yield RNA Transcription Kit	Ambion	Cat # AM1344
Phusion U Hot Start DNA polymerase	Thermo Fisher	Cat # F555
USER enzyme mix	New England Biolabs	M550
Experimental Models: Organisms/Strains		
Arabidopsis thaliana Col-0 wild-type	[10]	N/A

REAGENT or RESOURCE	SOURCE	IDENTIFIER
bak1–4	[10]	N/A
btl1 (*cngc20–3*)	ABRC	SALK _013823C
cngc1	ABRC	SAIL_443_B11
cngc2	[16]	*dnd1–1*
cngc3	ABRC	SALK_056832C
cngc4	[17]	*dnd2–1*
cngc5	ABRC	SALK_149893C
cngc6	ABRC	SALK_042207
cngc7	ABRC	SALK_060871C
cngc8	ABRC	GABI_101C03
cngc9	ABRC	SALK_026086
cngc10	ABRC	SALK_015952C
cngc11	ABRC	SALK_026568C
cngc12	ABRC	SALK_092657
cngc13	ABRC	SALK_060826
cngc14	ABRC	WiscDsLox437E09
cngc15	ABRC	CS93507
cngc16	ABRC	SAIL_726_B04
cngc17	ABRC	SALK_041923
cngc19	ABRC	SALK_007105
cngc20–1	ABRC	SALK_129133C
cngc20–2	ABRC	SALK_074919C
bak1–4	[10]	N/A
bak1–4/serk4–1	[10]	N/A
pepr1/2	[19]	N/A
bak1–4/cngc20–1	This paper	N/A
bak1–4/serk4–1/cngc20–3	This paper	N/A
bak1–4/serk4–1/cngc20–1	This paper	N/A
bak1–4/serk4–1/cngc20–1/cngc19	This paper	N/A
pCNGC20::gCNGC20-HA/cngc20–3	This paper	N/A
pCNGC20::gCNGC20$^{T560/S617/S618/T619D}$*-HA/cngc20–1*	This paper	N/A
p35S::CNGC20-HA/Col-0	This paper	N/A
p35S::CNGC20-HA/bak1–4	This paper	N/A
p35S::AT1G60995-HA/btl1	This paper	N/A
pAT1G60995::AT1G60995-HA/btl1	This paper	N/A
Xenopus laevis	[49]	N/A
Saccharomyces cerevisiae strain W303–1A	H Iida laboratory (Tokyo Gakugei University)	N/A
Saccharomyces cerevisiae strain K927	H Iida (Tokyo Gakugei University).	N/A

REAGENT or RESOURCE	SOURCE	IDENTIFIER
Saccharomyces cerevisiae strain AH109	[41]	N/A
Oligonucleotides		
Primers for VIGS, cloning and point mutation, see Table S4	This paper	N/A
Primers for genotyping, see Table S4	This paper	N/A
Primers for qRT-PCR and RT-PCR, see Table S4	This paper	N/A
Recombinant DNA		
pYL156 (*pTRV-RNA2*)	[10]	N/A
pTRV-RNA1	[10]	N/A
pYL156-GFP	[10]	N/A
pYL156-BAK1/SERK4	[10]	N/A
pYL156-MEKK1	[10]	N/A
pYL156-BIR1	[10]	N/A
pHBT	[41]	N/A
pGST	[45]	N/A
pMAL-c2	[45]	N/A
pCB302	[10]	N/A
pGADT7	[41]	N/A
pGBKT7	[41]	N/A
pNB1	[49]	N/A
pHEE401E	[47]	N/A
pCBC-DT1T2	[47]	N/A
pHBT-p35S::GCaMP3	This paper	N/A
pYES2	[34]	N/A
pHBT-BAK1-HA	[45]	N/A
pHBT-BIK1-HA	[45]	N/A
pHBT-BAK1-FLAG	[45]	N/A
pHBT-SERK4-FLAG	[45]	N/A
pMAL-BAK1^{CD}-HA	[45]	N/A
pMAL-BAK1^{CD}KM-HA	[45]	N/A
pHBT-CNGC20-HA	This paper	N/A
pHBT-CNGC20-FLAG	This paper	N/A
pHBT-CNGC20-cYFP	This paper	N/A
pHBT-CNGC19-HA	This paper	N/A
pHBT-CNGC19-nYFP	This paper	N/A
pHBT-CNGC20C-HA	This paper	N/A
pHBT-CNGC20N-FLAG	This paper	N/A
pHBT-CNGC20N$^{T145/S146/S183/S184A}$-HA	This paper	N/A
pHBT-CNGC20C^{T560A}-HA	This paper	N/A
pHBT-CNGC20C$^{T560/S617/S618/T619A}$-HA	This paper	N/A

REAGENT or RESOURCE	SOURCE	IDENTIFIER
pHBT-CNGC20C$^{T560/S617/S618/T619D}$-HA	This paper	N/A
pHBT-p35S::gCNGC20-HA	This paper	N/A
pHBT-pCNGC20::gCNGC20-HA	This paper	N/A
pGST-CNGC20N	This paper	N/A
pGST-CNGC20C	This paper	N/A
pGST-CNGC20N$^{T145/S146/S183/S184A}$	This paper	N/A
pGST-CNGC20C^{T560A}	This paper	N/A
pGST-CNGC20C$^{T560/S617/S618/T619A}$	This paper	N/A
pGADT7-BAK1^{K}	This paper	N/A
pGBKT7-CNGC20N	This paper	N/A
pCAMBIA1300-pCNGC20::gCNGC20-HA	This paper	N/A
pCAMBIA1300-pCNGC20::gCNGC20$^{T560/S617/S618/T619D}$-HA	This paper	N/A
pNB1YFP-CNGC19	This paper	N/A
pNB1YFP-CNGC20	This paper	N/A
pNB1YC-CNGC19	This paper	N/A
pNB1YN-CNGC20	This paper	N/A
pHEE401E-CNGC19	This paper	N/A
pCB302–35S::CNGC20-HA	This paper	N/A
pCB302-p35S::AT1G60995-HA	This paper	N/A
pCB302-pAT1G60995::AT1G60995-HA	This paper	N/A
pCB302-pBAK1::BAK1-FLAG	This paper	N/A
pYES2-CNGC19	This paper	N/A
pYES2-CNGC20	This paper	N/A
Software and Algorithms		
Bowtie aligner software	[50]	http://bowtie-bio.sf.net
CLC Genomics Workbench 6.0.1 software	QIAGEN	http://www.clcbio.com
LTQ Orbitrap XL LC-MS/MS system	Thermo Scientific	N/A
Mascot	Matrix Science	Version 2.2.2
Olympus Fluoview Viewer	Olympus	Version 3.0
ZEN	Zeiss	https://www.zeiss.com/microscopy/int/products/microscope-software/zen-lite.html
LAS-X	Leica	https://www.leica-microsystems.com/products/microscope-software/p/leica-las-x-ls/
ImageJ	NIH	https://imagej.nih.gov/ij/